

1 **Biogeochemical processes captured by carbon isotopes in**
2 **redox-stratified water columns: a comparative study of four**
3 **modern stratified lakes along an alkalinity gradient.**

4
5 Robin Havas^{a,*}, Christophe Thomazo^{a,b}, Miguel Iniesto^c, Didier Jézéquel^d, David Moreira^e, Rosaluz Tavera^e,
6 Jeanne Caumartin^f, Elodie Muller^f, Purificación López-García^e, Karim Benzerara^f
7

8 ^a Biogéosciences, CNRS, Université de Bourgogne Franche-Comté, 21000 Dijon, France

9 ^b Institut Universitaire de France, 75005 Paris, France

10 ^c Ecologie Systématique Evolution, CNRS, Université Paris-Saclay, AgroParisTech, 91190 Gif-sur-Yvette,
11 France

12 ^d IPGP, CNRS, Université de Paris, 75005 Paris, and UMR CARRTEL, INRAE & USMB, France

13 ^e Departamento de Ecología y Recursos Naturales, Universidad Nacional Autónoma de México, México

14 ^f Sorbonne Université, Muséum National d'Histoire Naturelle, CNRS, Institut de Minéralogie, de Physique des
15 Matériaux et de Cosmochimie (IMPMC), 75005 Paris, France.

16
17
18 * *Correspondence to:* Robin Havas (robin.havas@gmail.com)

19
20
21
22 *Keywords: Carbon cycle; DIC; POC; isotopic fractionation; Precambrian analogues*
23
24

25 **Abstract.** Redox-stratified water columns are a prevalent feature of Earth history, and ongoing environmental
26 changes tend to promote a resurgence of such settings. Studying modern redox-stratified environments has
27 improved our understanding of biogeochemical processes and element cycling in such water columns. These
28 settings are associated with peculiar carbon biogeochemical cycling owing to a layered distribution of biological
29 processes in relation to oxidant availability. Metabolisms from distinct biogeochemical layers are diverse and may
30 differently imprint the sedimentological record. Paired carbon isotope compositions of organic matter and
31 carbonates, which are commonly used to characterize these ecological dynamics, can thus vary from one stratified
32 environment to another. Changes in the organic/inorganic carbon sources and mass balance can further complicate
33 the isotopic message in stratified environments. Better understanding of these multifaceted carbon isotope signals
34 requires further evaluation of how the processes occurring in redox-stratified water columns are transferred to the
35 sediments. We therefore characterized and compared the isotopic signatures of dissolved inorganic carbon (DIC),
36 carbonate, and organic matter reservoirs, at different depths in the water column and upper sediments of four
37 stratified Mexican lakes that follow a gradient of alkalinity/salinity. Comparing these systems shows strong
38 diversity in the carbon isotope signals of the water column and sediments. Differences in inorganic carbon isotope
39 signatures arise primarily from the size of the DIC reservoir, buffering the expression of redox-dependent
40 biological processes as alkalinity increases. Combining this isotopic dataset with water-column physico-chemical
41 parameters allows us to identify oxygenic photosynthesis and aerobic respiration in the four lakes studied, while
42 anoxygenic photosynthesis is evidenced in only two of them. Sedimentary organic matter does not originate from
43 the same water-column layers in the four lakes, highlighting the ecological variability that can stem from different
44 stratified water columns, and how it is transferred or not to the sedimentary record. The least alkaline lake shows
45 higher isotopic variability, and signatures typical of methanogenesis in the sediment porewaters. This metabolism,
46 however, does not leave diagnostic isotopic signatures in the sedimentary archives (organic matter and carbonates),
47 underlining the fact that even when alkalinity does not strongly buffer the inorganic carbon reservoir, a
48 comprehensive picture of the active biogeochemical carbon cycling is not necessarily transferred to the geological
49 record.

50 1. INTRODUCTION

51 The carbon cycle and biogeochemical conditions prevailing at the surface of the Earth are intimately bound through
52 biological (e.g. photosynthesis) and geological processes (e.g. volcanic degassing and silicate weathering). The
53 analysis of carbon isotopes in organic matter and carbonates ($\delta^{13}\text{C}_{\text{org}}$ and $\delta^{13}\text{C}_{\text{carb}}$) in the rock record, has been used
54 to reconstruct the evolution of the biosphere and the oxygenation of the Earth's surface (e.g. Hayes et al., 1989;
55 Karhu and Holland, 1996; Schidlowski, 2001). Coupling $\delta^{13}\text{C}_{\text{org}}-\delta^{13}\text{C}_{\text{carb}}$ has frequently been used to infer the burial
56 rate of organic C, and thus the redox balance of the atmosphere and hydrosphere (e.g. Karhu and Holland, 1996;
57 Aharon, 2005; Krissansen-Totton et al., 2015; Mason et al., 2017). It has also been used to deduce the presence of
58 metabolisms like anoxygenic chemoautotrophic or methanotrophic bacteria (e.g. Hayes et al., 1999; Bekker et al.,
59 2008; Krissansen-Totton et al., 2015). Coupling $\delta^{13}\text{C}_{\text{org}}-\delta^{13}\text{C}_{\text{carb}}$ has also been used to discuss oceans stratification
60 and its effect on inorganic and organic C geochemical signatures in sediments (e.g. Logan et al., 1995; Aharon,
61 2005; Bekker et al., 2008; Ader et al., 2009). Stratification favors the expression and recording of different layers
62 of the water column, with potentially very distinct isotopic signatures. As the oceans were redox-stratified during
63 most of the Earth's history (Lyons et al., 2014; Havig et al., 2015; Satkoski et al., 2015), processes affecting the C
64 cycle were likely different from those occurring in most modern, well-oxygenated environments. This change of
65 conditions could impact the $\delta^{13}\text{C}_{\text{org}}$ signal at various scales, from changes in diversity and relative abundance of
66 microbial carbon and energy metabolism (e.g. Wang et al., 2016; Iñiguez et al., 2020; Hurley et al., 2021), to larger
67 ecological interactions (e.g. Jiao et al., 2010; Close and Henderson, 2020; Klawonn et al., 2021) and global C
68 dynamics (e.g. Ridgwell and Arndt, 2015; Ussiri and Lal, 2017).

69 Modern stratified lakes have been used as analogues of ancient redox-stratified systems to better understand the C
70 cycle in the sedimentary isotopic record (e.g. Lehmann et al., 2004; Posth et al., 2017; Fulton et al., 2018). Several
71 number of recent studies have investigated the C cycle in modern stratified water columns (e.g. Crowe et al., 2011;
72 Kuntz et al., 2015; Posth et al., 2017; Schiff et al., 2017; Havig et al., 2018; Cadeau et al., 2020; Saini et al., 2021;
73 Petrash et al., 2022), where many bio-geo-physico-chemical parameters can be directly measured, together with
74 the main C reservoirs. However, investigations of such Precambrian analogues do not necessarily include sediment
75 data, and generally focus on a single environment without integrating views from several systems.

76 In this study, we measured the concentrations and isotopic compositions of dissolved inorganic carbon (DIC) and
77 particulate organic carbon (POC) throughout the water column of four modern redox-stratified alkaline crater
78 lakes, located in the Trans-Mexican Volcanic Belt (Ferrari et al., 2012). We also measured the concentrations and
79 isotopic compositions of the sedimentary organic carbon and carbonates as well as porewater DIC from surficial
80 sediments (~ 10 cm) at the bottom of the lakes. The four lakes share similar geological and climatic contexts but
81 have distinct solution chemistries along a marked alkalinity–salinity gradient (Zeyen et al., 2021) – as well as
82 distinct planktonic communities (Iniesto et al., 2022). We therefore seek to evaluate how these environmental and
83 ecological differences are recorded in the C isotope signatures in the water columns (DIC–POC) and sedimentary
84 archives (organic matter–carbonates). The four lakes are closed lakes in endorheic basins (Alcocer, 2021; Zeyen
85 et al., 2021), which facilitates the identification of external environmental constraints (e.g. evaporation, C sources)
86 and their influence on processes occurring within the water columns. Depth profiles of the main physico-chemical
87 parameters together with trace and major elements concentrations were measured to pinpoint the dominant
88 biogeochemical processes occurring in the water columns and link them to specific C isotopes signatures.

89 First, we constrain the main DIC sources and external controls on the lakes' alkalinity. Next, we describe the
90 influence of the inter-lake alkalinity gradient on the inorganic C cycle and stratification of the lakes, and how it is
91 recorded in surficial sediments. Then, by combining POC and DIC data, we identify the sources of organic C to
92 the lakes by describing the main autotrophic reactions occurring in the water columns (e.g. oxygenic and
93 anoxygenic photosynthesis). Finally, we discuss the fate of POC, either recycled (e.g. via methanogenesis) or
94 deposited in the sediments, and how all these processes are recorded (or not) in surficial sediments.

95

96 **2. SETTING / CONTEXT**

97 **2.1. Geology**

98 The four lakes studied here are volcanic maars formed after phreatic, magmatic, and phreatomagmatic explosions,
99 related to volcanic activity in the Trans-Mexican Volcanic Belt (TMVB, Fig. 1). The TMVB originates from the
100 subduction of the Rivera and Cocos plates beneath the North America plate, resulting in a long (~1000 km) and
101 wide (90–230 km) Neogene volcanic arc spreading across central Mexico (Ferrari et al., 2012). The TMVB harbors
102 a large variety of monogenetic scoria cones and phreatomagmatic vents (maars and tuff-cones) as well as
103 stratovolcanoes, calderas, and domes (Carrasco-Núñez et al., 2007; Ferrari et al., 2012; Siebe et al., 2014). Maar
104 crater formation usually occurs when ascending magma meets water-saturated substrates, leading to successive
105 explosions and the excavation of older units (Lorenz, 1986; Carrasco-Núñez et al., 2007; Siebe et al., 2012; Chako
106 Tchamabé et al., 2020).

107 The first lake, La Alberca de los Espinos (1985 masl), is located at the margin of the Zacapu tectonic lacustrine
108 basin in the Michoacán-Guanajuato Volcanic Field (MGVF) in the central-western part of the TMVB (Fig. 1). It
109 lies on andesitic basement rocks and was dated at $\sim 25 \pm 2$ ka (Siebe et al., 2012, 2014). The other three lakes (La
110 Preciosa, Atexcac and Alchichica) are all in the same area (~ 50 km²) of the Serdan-Oriental Basin (SOB) in the
111 easternmost part of the TMVB (Fig. 1). The SOB is a closed intra-montane basin at high altitude (~ 2300 m),
112 surrounded by the Los Humeros caldera to the north and the Cofre de Perote-Citlatépel volcanic range to the east.
113 The basement is composed of folded and faulted Cretaceous limestones and shales, covered by andesitic-to-basaltic
114 lava flows (Carrasco-Núñez et al., 2007; Armienta et al., 2008; Chako Tchamabé et al., 2020). The Alchichica and
115 Atexcac craters was dated at $\sim 6\text{-}13 \pm 5\text{-}6$ ka (Chako Tchamabé et al., 2020) and 330 ± 80 ka (Carrasco-Núñez et
116 al., 2007), respectively (Table 1). The age of La Preciosa is not known.

117

118 **2.2. Climate and limnology**

119 La Alberca is a freshwater lake (0.6 psu) with a temperate to semi-humid climate (Rendon-Lopez, 2008; Sigala et
120 al., 2017). In contrast, lakes from the SOB experience a similar temperate to semi-arid climate (Armienta et al.,
121 2008; Sigala et al., 2017). The current climate of the SOB is dominated by dry conditions, reflected by higher
122 evaporation than precipitation fluxes in Lake Alchichica (~ 1686 vs. 392 mm/year; Alcocer, 2021). In La Preciosa,
123 Atexcac, and Alchichica, significant evaporation is reflected by a drop in water level, evidenced by the emersion
124 of microbialite deposits (Fig. S1; Zeyen et al., 2021). This evaporation-dominated climate strongly contributes to
125 the relatively high salinity values in these lakes (1.2–7.9 psu), ranging from sub- to hyposaline.

126 The four lakes are warm monomictic: they are stratified for about nine months of the year, mixing only when
127 thermal stratification breaks down in the cold of winter (Armienta et al., 2008). They are all closed lakes located
128 in an “endorheic” basin (Alcocer, 2021; Zeyen et al., 2021), meaning that they have no inflow, outflow, or
129 connection to other basins through surficial waters such as streams. The only water input is from precipitation and
130 groundwater inflow (quantified for Lake Alchichica; Alcocer, 2021 and references therein).

131 The four lakes are alkaline (pH ~ 9) but cover a broad range of chemical compositions (including alkalinity,
132 salinity, and Mg/Ca ratio), interpreted as reflecting different concentration stages of an initial alkaline dilute water
133 (Table 1; Zeyen et al., 2021). Variations in concentration stages may be due to differences in climate and, more
134 generally, different hydrological regimes. Microbialite deposits are found in all four lakes (Gérard et al., 2013;
135 Saghaï et al., 2016; Iniesto et al., 2021a, 2021b; Zeyen et al., 2021), and increase in abundance from lower to
136 higher alkalinity conditions (Zeyen et al., 2021).

137

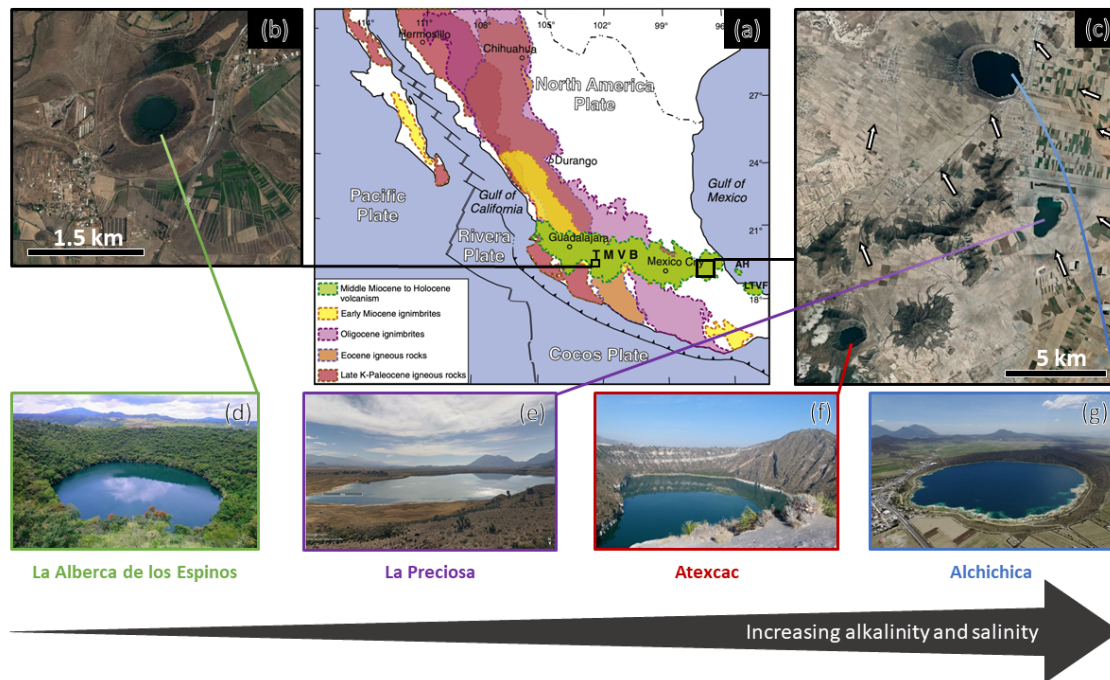
138 **3. METHOD**

139 **3.1. Sample Collection**

140 The sediment core from Lake La Preciosa was collected in May 2016. All other samples were collected in May
141 2019. The depth profiles of several physico-chemical parameters were measured in the water columns of the four
142 lakes using an YSI Exo 2 multi-parameter probe: temperature, pH, ORP (oxidation reduction potential),
143 conductivity, O₂, chlorophyll a, phycocyanin, and turbidity. Precisions for these measurements were 0.01 °C, 0.1
144 pH unit, 20 mV, 0.001 mS/cm, 0.1 mg/L, 0.01 µg/L, 0.01 µg/L and 2% FTU unit, respectively. The ORP signal
145 was not calibrated before each profile and is thus used to discuss relative variations over a depth profile.
146 Measurements of the aforementioned parameters served to pinpoint depths of interest for further chemical and
147 isotopic analyses, notably around the redoxcline of the lakes. Water samples were collected with a Niskin bottle.
148 Particulate matter was collected on pre-combusted (2 h at 490°C) and weighted glass fiber filters (Whatman GF/F,
149 0.7 µm) and analyzed for particulate organic carbon (POC), major and trace elements. Between 1.5 and 5 L of lake
150 water was filtered before the GF/F filters became clogged. The processed solution was filtered again at 0.22 µm
151 with Filtropur S filters (pre-rinsed with lake water filtered at 0.7 µm) for analyses of dissolved inorganic carbon
152 (DIC), and major, minor, and trace ions.

153 Sediment cores were collected using a 90 mm Uwitec corer close to the deepest point of each lake’s water column
154 (Table 1), where anoxic conditions prevail almost all year long. Cores measured between 20 and 85 cm in length.
155 Slices of about 2-3 cm were cut under anoxic conditions, using a glove bag filled with N₂ (anoxia was monitored
156 using a WTW3630 equipped with a FDO O₂ optode). Interstitial porewater was drained out of the core slices using
157 Rhizons in the glove bag. Sediments were transported back to the laboratory within aluminized foils (Protpack,
158 UK). Sediments were then fully dried in a laboratory anoxic N₂-filled glove box.

159



160 Figure 1. Geographical location and photographs of the four crater lakes. (a) Geological map from Ferrari et al.
 161 (2012) with black squares showing the location of the four studied lakes within the Trans-Mexican Volcanic Belt
 162 (TMVB). (b, c) Close up © Google Earth views of La Alberca de los Espinos and the Serdan-Oriental Basin
 163 (SOB). The white arrows represent the approximate groundwater flow path (based on Silva-Aguilera, 2019). (d-
 164 g) Photographs of the four lakes (d from © Google Image [‘enamoredemexicowebiste’], e from © Google Earth
 165 street view, and g from © ‘Agencia Es Imagen’).

166

Lake	General location	Sampling location	Elevation (masl)
Alchichica	Serdan Oriental Basin, eastern TMVB	19°24'51,5" N; 97°24'09,9" W	2320
Atexcac	Serdan Oriental Basin, eastern TMVB	19°20'2.2" N; 97°26'59.3" W	2360
La Preciosa	Serdan Oriental Basin, eastern TMVB	19°22'18.1" N; 97°23'14.4" W	2330
La Alberca de los Espinos	Zacapu Basin, MGVF, central TMVB	19°54'23.9" N; 101°46'07.8" W	1985

167

Lake	Lake Basement	Age	Max Depth (m)	Alkalinity (mmoles/L)	Salinity (psu)	pH
Alchichica	limestone, basalts	6-13 ± 5-6 ka	63	~35	7.9	9.22
Atexcac	limestone, andesites, basalts	330 ± 80 ka	39	~26	7.4	8.85
La Preciosa	limestone, basalts	Pleistocene	46	~13.5	1.15	9.01
La Alberca de los Espinos	andesite xenoliths	25 ± 2 ka	30	~7	0.6	9.14

168

169 Table 1. General information about the lakes studied. Abbreviations: TMVB: Trans-Mexican Volcanic Belt;
 170 MGVF: Michoacán-Guanajuato Volcanic Field; masl.: meters above sea level. NB: Sampling took place in
 171 May 2019, except for La Preciosa sediments, sampled in May 2016.

172 **3.2. Dissolved inorganic carbon (DIC) concentration and isotope measurements**

173 Twelve mL of the 0.7- μm filtered lake water was filtered at 0.22- μm directly into hermetic Exetainer® tubes to
174 avoid exchange between DIC and atmospheric CO_2 . The DIC concentrations and isotopic compositions were
175 measured at the Institut de Physique du Globe de Paris (IPGP, France), using an Analytical Precision 2003 GC-
176 IRMS, running under He-continuous flow, following the protocol described by Assayag et al. (2006). A given
177 volume of the solution was extracted from the Exetainer® tube with a syringe, while the same volume of helium
178 was introduced to maintain stable pressure and atmospheric- CO_2 -free conditions within the sample tubes. The
179 collected sample was inserted into another Exetainer® tube, pre-filled with a few drops of 100% phosphoric acid
180 (H_3PO_4) and pre-flushed with He gas. Under acidic conditions, DIC quantitatively converts to gaseous and aqueous
181 CO_2 , which equilibrates overnight within the He-filled head space of the tube. Quantification and isotopic analyses
182 of released gaseous CO_2 were then carried out by GC-IRMS using internal standards of known composition that
183 were prepared and analyzed via the same protocol. Each measurement represented an average of four injections in
184 the mass spectrometer. Chemical preparation and IRMS analysis were duplicated for all the samples. The $\delta^{13}\text{C}_{\text{DIC}}$
185 reproducibility calculated for the 65 samples was better than ± 0.2 ‰, including internal and external
186 reproducibility. Standard deviation for [DIC] was 0.6 ± 0.9 mmol/L on average.

187 Specific DIC speciation, i.e., $\text{CO}_{2(\text{aq})}$, HCO_3^- and CO_3^{2-} activities, was computed using Phreeqc with the full
188 dissolved chemical composition of each sample as an input. It should be noted that these results are calculated
189 from theoretical chemical equilibria and do not necessarily take into account local kinetic effects, which, for
190 example, could lead to local exhaustion of $\text{CO}_{2(\text{aq})}$ where intense photosynthesis occurs.

191

192 **3.3. Particulate organic carbon and nitrogen (POC / PON)**

193 Particulate organic matter from the lake water columns was collected on GF/F filters, dried at room temperature
194 and ground in a ball mill before and after decarbonation. Decarbonation was performed with 12N HCl vapors in a
195 desiccator for 48 h. Aliquots of dry decarbonated samples (25 - 70 mg) were weighed in tin capsules. The POC
196 and PON contents and $\delta^{13}\text{C}_{\text{POC}}$ were determined at the Laboratoire Biogéosciences (Dijon, France) using a Vario
197 MICRO cube elemental analyzer (Elementar, Hanau, Germany) coupled in continuous flow mode with an
198 IsoPrime IRMS (Isoprime, Manchester, UK). The USGS 40 and IAEA 600 certified materials used for calibration
199 showed reproducibility better than 0.15 ‰ for $\delta^{13}\text{C}$. External reproducibility based on triplicate analyses of
200 samples (n=23) was 0.1 ‰ on average for $\delta^{13}\text{C}_{\text{POC}}$ (1SD). External reproducibility for POC and PON
201 concentrations was 0.001 and 0.005 mmol/L on average, respectively (i.e. 3 and 7 % of measured concentrations).

202

203 **3.4. Geochemical characterizations of the sediments**

204 Sedimentary organic carbon (SOC), sedimentary organic nitrogen (SON), and their isotopic compositions were
205 measured on carbonate-free residues of the first 12 cm of the sediment cores, produced after overnight 1N HCl
206 digestion. Plant debris (mainly found in La Alberca and Atexcac) was identified upon initial sediment grinding in
207 an agate mortar and analyzed separately. Aliquots of dried decarbonated samples (~ 4-70 mg) were weighed in tin
208 capsules. The SOC and SON contents and $\delta^{13}\text{C}$ were determined at the Laboratoire Biogéosciences (Dijon) using

209 a Vario MICRO cube elemental analyzer (Elementar GmbH, Hanau, Germany) coupled in continuous flow mode
210 with an IsoPrime IRMS (Isoprime, Manchester, UK). The USGS 40 and IAEA 600 certified materials used for
211 calibration had a reproducibility better than 0.2 ‰ for $\delta^{13}\text{C}_{\text{SOC}}$. Sample analyses (n=67) were at least duplicated
212 and showed an average external reproducibility of 0.1 ‰ for $\delta^{13}\text{C}$ (1SD). External reproducibility for SOC and
213 SON contents was 0.1 and 0.03 wt. %, respectively.

214 Carbon isotope compositions of sedimentary carbonates were analyzed at the Laboratoire Biogéosciences (Dijon)
215 using a ThermoScientific™ Delta V Plus™ IRMS coupled with a Kiel VI carbonate preparation device. External
216 reproducibility was assessed by multiple measurements of NBS19 standard and was better than ± 0.1 ‰ (2σ).
217 Total carbonate concentration was determined by mass balance after decarbonation for SOC analysis.

218 Mineralogical assemblages of sediments were determined on bulk powders by X-Ray diffraction (XRD) at the
219 Laboratoire Biogéosciences (Dijon). Samples were ground in an agate mortar. Diffractograms were obtained with
220 a Bruker D8 Endeavor diffractometer with $\text{CuK}\alpha$ radiation and LynxEye XE-T detector, under 40 kV and 25 mA
221 intensity. Mineral identification was based on COD (“Crystallography Open Database”) and BGMN databases.
222 Mineral abundances were estimated by Rietveld refinement analysis implemented in the Profex software.

223 Solid sulfide concentrations were determined on dry bulk sediments from La Alberca Lake after a wet chemical
224 extraction using a boiling acidic Cr(II)-solution as detailed in Gröger et al. (2009).

225

226 **3.5. Major and trace elements concentrations**

227 Dissolved and particulate matter elemental compositions were measured at the Pôle Spectrométrie Océan
228 (Plouzané, France) by inductively coupled plasma–atomic emission spectroscopy (ICP-AES, Horiba Jobin) for
229 major elements and by high-resolution ICP–mass spectrometry using an Element XR (HR-ICP-MS, Thermo Fisher
230 Scientific) for trace elements. Major element measurement reproducibility based on internal multi-elemental
231 solution was better than 5%. Trace elements were analyzed by a standard-sample bracketing method and calibrated
232 with a multi-elemental solution. Analytical precision for trace elements was generally better than 5%. Dissolved
233 sulfate concentrations were analyzed by ion chromatography at the IPGP (Paris, France) with uncertainty lower
234 than 5%.

235

236 **4. RESULTS**

237

238 **4.1. Lake La Alberca de los Espinos**

239 Stratification of the water column was well defined in La Alberca de los Espinos (Fig. 2). Temperature was higher
240 than in the other lakes (decreasing from ~ 23 °C at the surface to 16.5 °C at depth). Dissolved O_2 was oversaturated
241 at the lake surface (118 %, *i.e.*, 7.9 mg/L), rapidly decreasing to 0 between ~ 5 and 12 m, while the oxidation
242 reduction potential (ORP) only decreased below 17 m depth. The offset between O_2 exhaustion and ORP decrease
243 can be explained by the presence of other oxidant species and/or extended chlorophyll a peaks (supplementary
244 text 1). Conductivity decreased from 1.20 to 1.17 mS/cm at 16 m before increasing to 1.27 mS/cm at 26 m (salinity

245 between 0.58 and 0.64 psu). Chlorophyll a (Chl a) averaged 3.1 $\mu\text{g/L}$, and showed a profile with at least three
246 distinctive peaks, (i) between 6 and 9.5 m, (ii) around 12.5 m and (iii) between 16 and 19 m, all reaching $\sim 4 \mu\text{g/L}$.
247 The turbidity profile showed a pronounced increase from 16 to 19 m. The pH profile showed important variation
248 from 9.15 at the lake surface to 8.75 between 6.5 and 10 m, further decreasing to 7.5 between 16 and 26 m. Based
249 on the temperature profiles, epi-, meta- and hypolimnion layers of Lake La Alberca de los Espinos in May 2019
250 broadly extended from 0-5, 5-12 and 12-30 m, respectively (Fig. 2). The conductivity and pH profiles, however,
251 show that different conditions prevail at the top and bottom of the hypolimnion.

252 Dissolved inorganic carbon (DIC) concentration progressively increased from 6.8 mM at 5 m to 8.7 mM at 26 m.
253 The pCO_2 calculated for surface waters was near equilibrium with atmospheric $\text{pCO}_{2\text{atm}}$, but strongly increased
254 with depth, up to ~ 40 times the $\text{pCO}_{2\text{atm}}$ (Table S2). The $\delta^{13}\text{C}_{\text{DIC}}$ first decreased from about -2.5‰ to -4.1‰
255 between 5 and 10 m, before increasing again up to -2‰ at 25 m. Particulate organic carbon (POC) concentrations
256 reached minimum values of 0.02 mM at 10 m but rose to maximum values in the hypolimnion (0.06 mM). The
257 C:N molar ratio of particulate organic matter (POM) progressively decreased from 8.5 at the surface to less than
258 6.5 in the hypolimnion. The $\delta^{13}\text{C}_{\text{POC}}$ had minimum values at 10 and 17 m (-28.3 and -29‰ , respectively). Above
259 and below these depths, $\delta^{13}\text{C}_{\text{POC}}$ averaged $-26.4 \pm 0.5 \text{‰}$.

260 Dissolved sulfates as measured by chromatography were only detectable at 5 m with a low concentration of 12 μM ,
261 while total dissolved S measured by ICP-AES, showed values in the hypolimnion higher than in the upper layers
262 (~ 10.3 vs. $7.4 \mu\text{M}$, Table S4). Dissolved Mn concentrations decreased from 1.5 to 0.5 μM between 5 and 10 m,
263 then increased to 2 μM at 25 m. Aqueous Fe was only detectable at 25 m with a concentration of 0.23 μM
264 (Table S4). In parallel, particulate S concentrations increased with depth, with a marked increase from 0.1 to
265 0.6 μM between 20 and 25m. Increase in particulate S was correlated with a 25-fold increase in particulate Fe
266 (from 0.2 to 5.97 μM). Particulate Mn showed a peak between 17 and 20 m around 1 μM , contrasting with values
267 lower than 0.15 μM in the rest of the water column (Fig. 2, Table S5).

268 In the first centimeters of sediments, DIC concentration in the porewater varied between ~ 11 and 12 mM and
269 $\delta^{13}\text{C}_{\text{DIC}}$ varied between $+8$ and $+10 \text{‰}$ (Figs. 3, 4). Surficial sedimentary carbonates corresponded to calcite and
270 had a $\delta^{13}\text{C}$ around -1.5‰ . Sedimentary organic matter had a $\delta^{13}\text{C}_{\text{SOC}}$ increasing from ~ -29.4 to -25.5‰ and a
271 C:N molar ratio varying between 11.6 and 14.3 (Figs. 3, 4; Table S3).

272

273 4.2. Lake La Preciosa

274 Lake La Preciosa was also stratified at the time of sample collection (Fig. 2). Temperature decreased from $\sim 20 \text{°C}$
275 at the surface to 16°C at 15m depth. Conductivity showed the same trend with values between 2.24 and
276 2.22 mS/cm (salinity around 1.15 psu). Dissolved O_2 was oversaturated at the lake surface (120 %, i.e., 8.4 mg/L),
277 rapidly decreasing to 0 between ~ 8 and 14 m, while the ORP decreased right below 16 m. Chl a concentration
278 averaged 3 $\mu\text{g/L}$ and recorded the highest peak compared to the other lakes (about 9 $\mu\text{g/L}$ at 10 m) before
279 decreasing to 0.7 $\mu\text{g/L}$ below 15 m. Turbidity showed a large peak between 16 and 19 m. The pH showed a small
280 decrease from 9 to 8.8 between the surface and 15 m depth. Based on the temperature profiles, epi-, meta- and
281 hypolimnion layers of La Preciosa in May 2019 broadly extended from 0-6, 6-15 and 15-46 m, respectively
282 (Fig. 2).

283 The DIC concentration was constant throughout the water column at 13.3 mM, with an exception at 12.5 m, where
 284 it decreased to 11.5 mM (Fig. 3, Table S1). Calculated pCO₂ at the surface represented about two times the
 285 atmospheric pCO_{2atm} (Table S2). The δ¹³C_{DIC} decreased from about 0.5 ‰ to -0.36 ‰ between the surface and the
 286 hypolimnion. The POC concentration decreased from ~0.06 mM in the epi-/metalimnion to 0.02 mM in the
 287 hypolimnion. Similarly, (C:N)_{POM} decreased from ~11.2 in the epi-/metalimnion to 7.6 in the hypolimnion. The
 288 δ¹³C_{POC} increased downward from ~ -27 to -25 ‰ to with a peak to -23.5 ‰ at 15 m.

289 In the first 10 cm of sediments, δ¹³C_{SOC} values increased downwards from ~ -25.5 to -23.2 ‰ and C:N molar ratio
 290 from 9.8 to 11 (Figs. 3, 4; Table S3). Carbonates corresponded to aragonite and calcite and had a bulk C isotope
 291 composition averaging 2.6 ‰ (Table S3). Porewaters from the 2016 La Preciosa core were not retrieved.

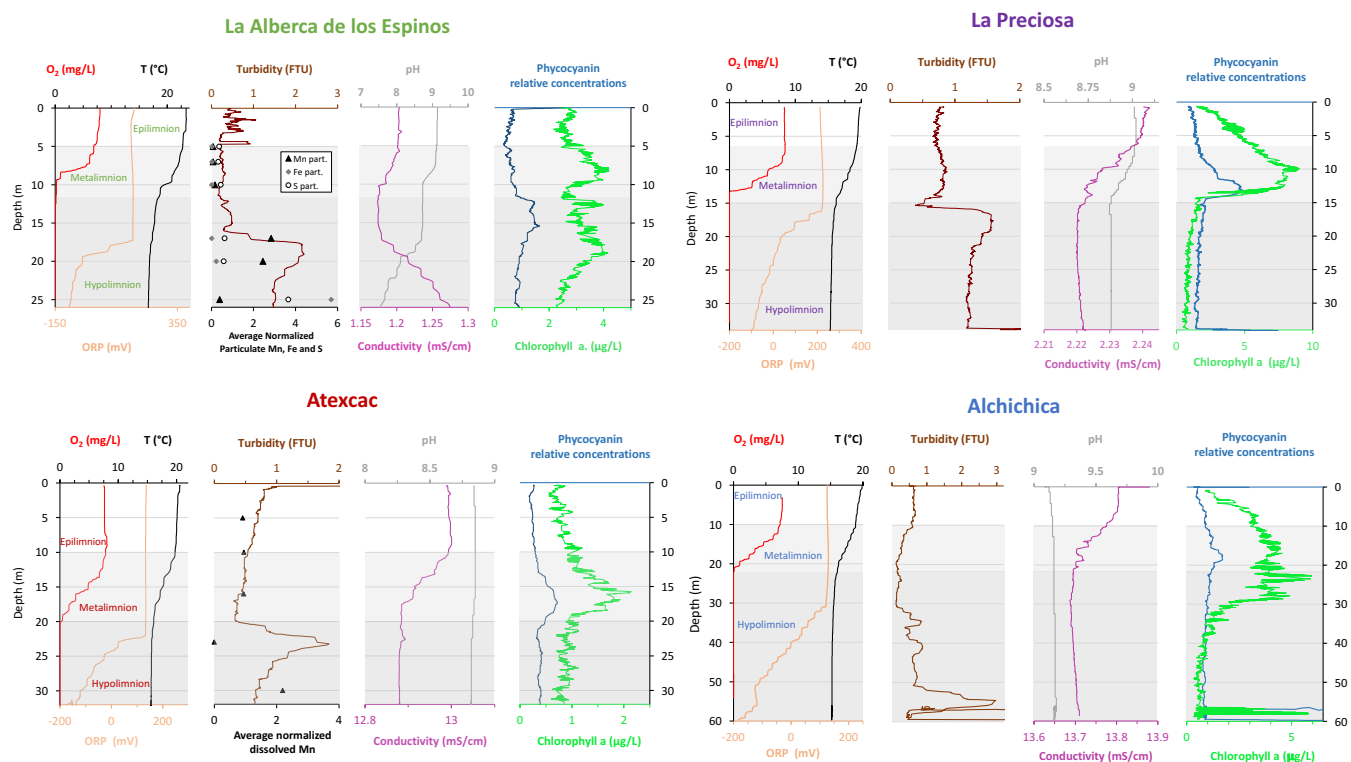


Figure 2. Physico-chemical parameters depth profiles in La Alberca de los Espinos , La Preciosa, Atexcac and Alchichica in May 2019 including: dissolved oxygen concentration (mg/L), water temperature (°C), oxidation-reduction potential (ORP, mV), turbidity (Formazin Turbidity Unit), pH, conductivity (mS/cm), phycocyanin and chlorophyll a pigments (µg/L). Absolute values for phycocyanin concentrations were not determined; only relative variations are represented (with increasing concentrations to the right). Discrete concentration values of dissolved Mn in Atexcac and particulate Mn, Fe and S in La Alberca, normalized by their respective average are represented. Epi-, meta- and hypo-limnion layers are depicted for each lake according to temperature profiles. The three layers closely corresponded to oxygen-rich, oxygen-poor and intermediate zones (except in La Preciosa where the oxycline was slightly thinner than the thermocline layer, ~5 vs. 8 m).

292

293 **4.3. Lake Atexcac**

294 Stratification of the Lake Atexcac water column was also very well defined (Fig. 2). Temperature decreased from
 295 ~ 20.6 °C at the surface to reach 16 °C below 20 m. Conductivity showed the same trend with values between 13
 296 and 12.8 mS/cm near the surface (salinity around 7.4 psu). Dissolved O₂ was slightly oversaturated at the lake

297 surface (115 % or 7.6 mg/L), rapidly decreasing to 0 mg/L between ~ 10 and 20 m, while ORP signal decreased
298 below a depth of 22 m. Chl a averaged 1 µg/L and showed a narrow peak centered at around 16 m, reaching
299 ~2 µg/L. Turbidity showed a pronounced increase below 20 m, peaking at 23.3 m and returning to surface values
300 at 26 m. The pH remained around 8.85 throughout the water column. Based on the temperature profiles, the epi-,
301 meta- and hypolimnion of Atexcac in May 2019 broadly extended from 0-10, 10-20 and 20-39 m, respectively
302 (Fig. 2).

303 The DIC concentration was around 26 mM throughout the water column, except at 23 m where it decreased to
304 24.2 mM (Fig. 3, Table S1). Calculated pCO₂ was about five times higher than the atmospheric pCO_{2atm} (Table S2).
305 The δ¹³C_{DIC} was stable around 0.4 ‰ in the epi-/metalimnion, but increased to 0.9 ‰ at 23 m and reached 0.2 ‰
306 minimum values at the bottom of the lake. The POC concentration was ~ 0.05 mM in the epi-/metalimnion,
307 decreasing to 0.02 mM in the hypolimnion. The C:N molar ratio of POM showed the same depth profile, decreasing
308 from ~9.6 in the epi-/metalimnion to 6.6 in the hypolimnion (Fig. 3). The δ¹³C_{POC} showed minimum values in the
309 epi-/metalimnion (-29.3 ‰ at 16 m) and increased to -26.5 ‰ in the hypolimnion.

310 Dissolved sulfate concentration was relatively stable at ~ 2.51 mM throughout the water column but increased to
311 2.64 mM at 23 m. Dissolved Mn concentration was constant at 1 µM down to 16 m before dropping to 0 at 23 m,
312 and increasing again to 2.35 µM at 30 m (Fig. 2; Table S4). Similar depth profiles were found for other heavy
313 elements as well, including Cu, Sr, Ba or Pb among others.

314 In the first 12 cm of sediments, DIC concentration in the porewater varied between ~ 21 and 26 mM, and δ¹³C_{DIC}
315 was around 0 ‰. Carbonates corresponded to aragonite and calcite and had a bulk C isotope composition between
316 2.1 and 2.6 ‰ (Table S3). Sedimentary organic matter had a δ¹³C_{SOC} averaging -26.8 ± 0.1 ‰ and a C:N molar
317 ratio increasing from 8 to 10 (Figs. 3, 4; Table S3).

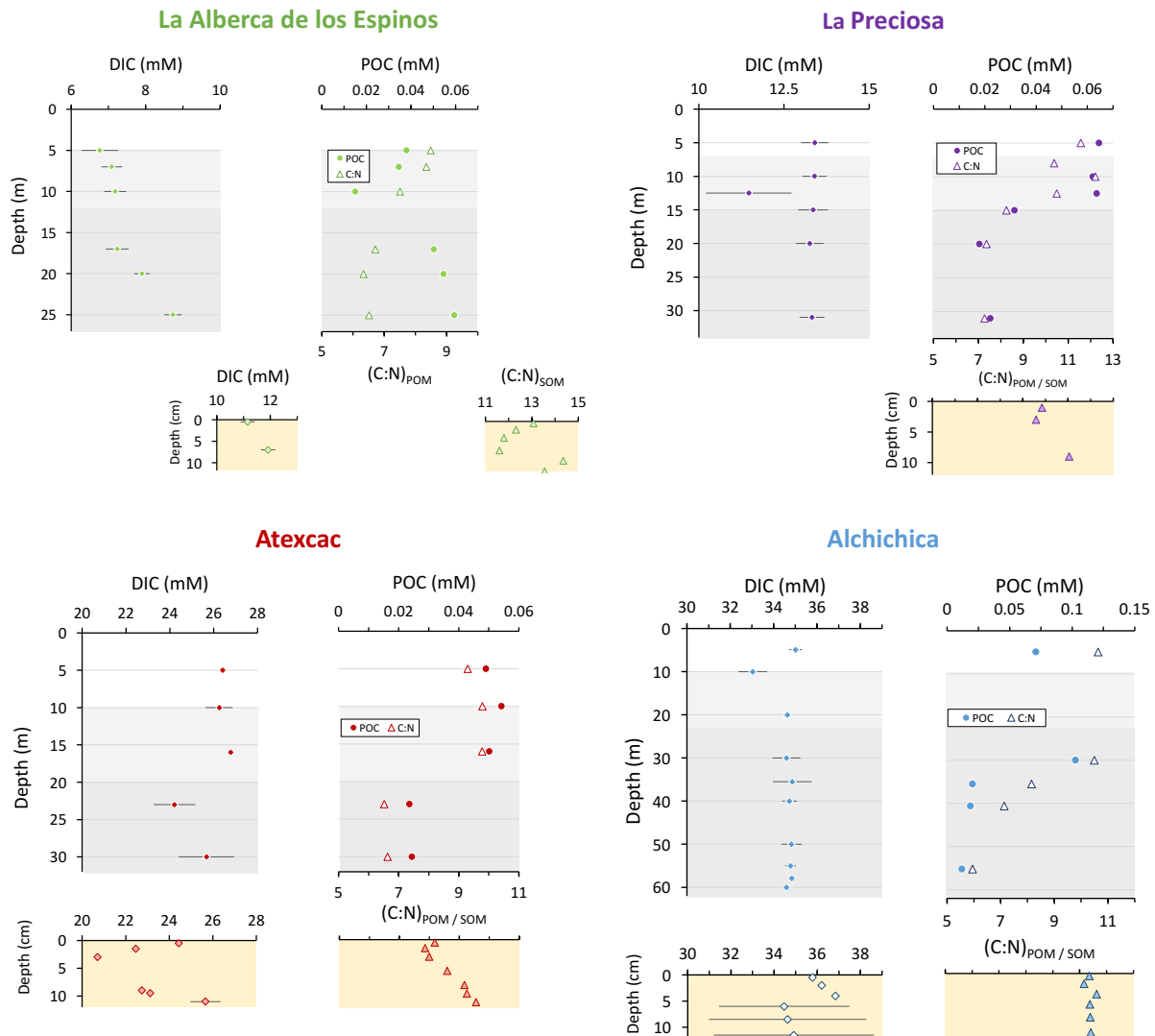


Figure 3. Concentrations in mmol/L (mM) of DIC, DOC, POC and sum of all three reservoirs, C:N molar ratios of POM as a function of depth in the water columns, as well as DIC concentrations in the surficial sediment porewaters and C:N molar ratios of sedimentary OM. Porewaters from La Preciosa's 2016 core were not retrieved.

318

319 4.4. Lake Alchichica

320 The water column of Lake Alchichica showed a pronounced stratification compared to previous years at the same
 321 period (Fig. 2, Fig. S2; Lugo et al., 2000; Adame et al., 2008; Macek et al., 2020). Temperature decreased from
 322 ~ 20 °C at the surface to 15.5 °C at depths below 30 m. Conductivity showed the same trend with values between
 323 around 13.8 mS/cm (salinity decreasing from 7.9 to 7.8 psu). Dissolved O₂ was slightly oversaturated at the lake
 324 surface (112 % or 7.5 mg/L), rapidly decreasing to 0 mg/L between ~ 10 and 20 m. The ORP followed a similar
 325 trend but decreasing below 30 m only. The offset between O₂ exhaustion and decrease of the ORP can be explained
 326 by the presence of other oxidant species and/or extended Chl a peaks (supplementary text 1). Chl a averaged
 327 2 µg/L, with a broad peak extending from ~ 7 to 29 m (averaging 4 µg/L and showing a narrow 6 µg/L maximum
 328 values at 23 m). Then, it decreased to minimum values of ~ 0.5 µg/L in the lower water column. The pH remained
 329 constant at ~9.2 over the whole water column. Based on the temperature profiles, the epi-, meta- and hypolimnion
 330 layers of Lake Alchichica in May 2019 extended from 0-10, 10-20 and 20-63 m, respectively (Fig. 2).

331 The DIC concentration was around 34.8 mM throughout the water column, except at 10 m where it decreased to
 332 33 mM (Fig. 3; Table S1). Calculated pCO₂ was about three times higher than the atmospheric pCO_{2atm} (Table S2).
 333 The δ¹³C_{DIC} decreased from 2 to ~ 1.5 ‰ between 5 and 60 m depth (Fig. 4; Table S1). The POC concentration
 334 was ~ 0.09 mM in the epi-/metalimnion, decreasing to 0.02 mM in the hypolimnion. The δ¹³C_{POC} increased from
 335 -26.5 ‰ in the top 30 m to -24.1 ‰ at 55 m. The C:N molar ratio of POM showed a similar profile with values
 336 around 10.5 down to 30 m, progressively decreasing towards 5.9 at 55 m (Fig. 3; Table S1).

337 In the first 12 cm of sediments, porewater DIC had a concentration of ~ 35.5 mM and δ¹³C_{DIC} decreased from 0.4
 338 to -0.5 ‰. Solid carbonates were contained within several phases (aragonite, hydromagnesite, huntite and calcite)
 339 and had a bulk C isotope composition around 4.6 ‰ (Table S3). Sedimentary organic matter had a δ¹³C_{SOC}
 340 increasing from -25.7 to -24.5 ‰ and a constant C:N molar ratio slightly higher than 10 (Figs. 3, 4; Table S3).

341

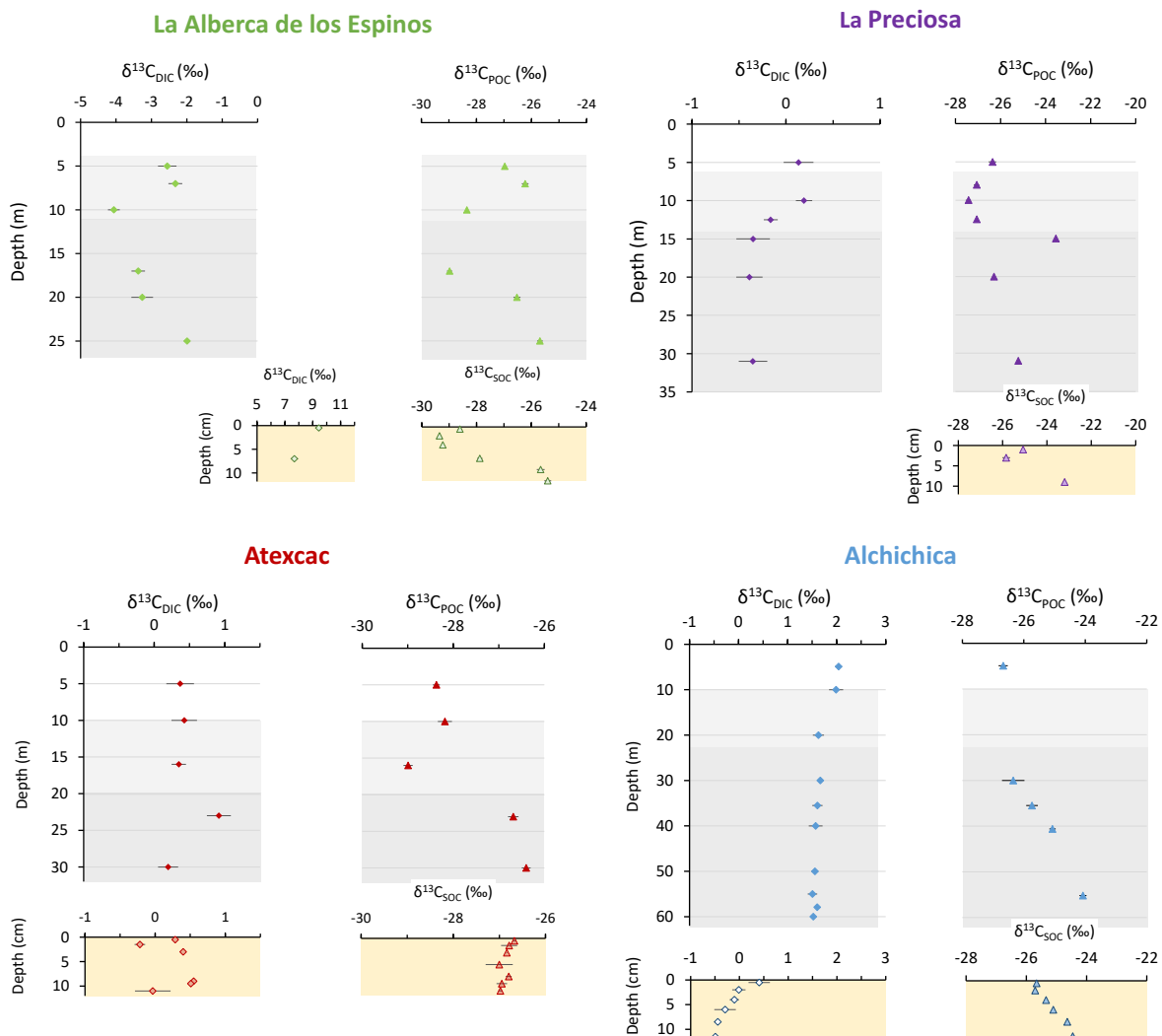


Figure 4. Isotopic compositions of DIC and POC reservoirs as a function of depth in the water columns, as well as isotopic compositions of the porewater-DIC and total organic carbon from the surficial sediments.

343 5. DISCUSSION

344 5.1. Inorganic Carbon: origins and implications of the alkalinity/DIC gradient

345 5.1.1 Sources of DIC and origin of the inter-lake alkalinity gradient

346 Salinity and DIC concentration gradually increase from La Alberca de los Espinos (0.6 psu, 7 mM) to Alchichica
347 (7.9 psu, 35 mM), while La Preciosa (1.15 psu, 13 mM) and Atexcac (7.44 psu, 26 mM) have intermediate values
348 (Table 1 and S1). This trend matches the alkalinity gradient (with values of ~ 8, 15, 32 and 47 meq/L, Fig. S3a)
349 previously described for these lakes (Zeyen et al., 2021), consistent with the fact that alkalinity is mainly composed
350 of HCO_3^- and CO_3^{2-} ions in most natural waters. This alkalinity gradient may result from different concentration
351 stages of an initial dilute alkaline water (Zeyen et al., 2021), ultimately controlled by differences in hydrological
352 regime between the four lakes. In the SOB, the weathering of basaltic/andesitic bedrock (Armienta et al., 2008;
353 Carrasco-Núñez et al., 2007; Lelli et al., 2021) and Cretaceous limestone (with $\delta^{13}\text{C} \approx 0 \pm 1 \text{‰}$; Gonzales-Partida
354 et al., 1993; Armstrong-Altrin et al., 2011) favors the inflow of more alkaline and DIC-concentrated groundwater
355 than in La Alberca, which lies on an essentially basaltic basement (Rendon-Lopez, 2008; Siebe et al., 2014; Zeyen
356 et al., 2021). The SOB is currently experiencing higher rates of evaporation than precipitation (Alcocer, 2021),
357 which may play an important role in concentrating solutes and decreasing the water level in La Preciosa, Atexcac,
358 and Alchichica (Anderson and Stedmon, 2007; Zeyen et al., 2021). Substantial “sub-fossil” microbialite deposits
359 emerge well above the current water level in lakes Atexcac and Alchichica, confirming this fall in water level
360 (~15 m for Atexcac, and ~5 m for Alchichica). Scattered patches of microbialites emerge at La Preciosa
361 (suggesting a water level decrease of ~6 m). By contrast, emerged microbialites are virtually absent in Lake La
362 Alberca de los Espinos (Fig. S1).

363 Additional local parameters such as variable groundwater paths and fluxes (Furian et al., 2013; Mercedes-Martín
364 et al., 2019; Milesi et al., 2020; Zeyen et al., 2021) most likely play a role in explaining some of the variation in
365 DIC concentration between lakes. La Preciosa’s water composition significantly differs from that of Atexcac, and
366 Alchichica, despite a similar geological context and climate (all are located within 50 km², Fig. 1). Groundwater
367 in the SOB area becomes more saline as it flows towards the center of the basin and through the crater lakes (Silva
368 Aguilera, 2019; Alcocer, 2021). Since groundwater flows through La Preciosa first, its ionic strength (including
369 DIC concentration) increases as it enters Alchichica (Silva Aguilera, 2019; Alcocer, 2021; Lelli et al., 2021).
370 Different regimes of volcanic CO₂ degassing into these crater lakes may also contribute to variation in the C mass
371 balance and $\delta^{13}\text{C}_{\text{DIC}}$ values between the four lakes. Near the lakes from the SOB area, geothermal fluids derived
372 from meteoric waters have been shown to interact with deep volcanic fluids as well as the calcareous basement
373 rocks (Peiffer et al., 2018; Lelli et al., 2021). In the water column of La Alberca, $\delta^{13}\text{C}_{\text{total}}$ averages -4.8 ‰ (Havas
374 et al., submitted). This isotopic composition is very similar to signatures of mantle-CO₂ (Javoy et al., 1986; Mason
375 et al., 2017), which could buffer the overall C isotope composition of this lake. La Alberca is located on top of a
376 likely active normal fault (Siebe et al., 2012), favoring the ascent of volcanic gases.

377 Differences in the remineralization rate of organic carbon (OC) could also contribute to the heterogeneous DIC
378 content among the lakes. However, assuming that all OC from the lakes ultimately remineralized into DIC, it
379 would still represent only a small proportion of the total carbon (9 % for La Alberca, ~5 % for La Preciosa and
380 Alchichica, and 16 % for Atexcac, Havas et al., submitted). From an isotopic mass balance perspective, Lake La
381
382

383 Alberca exhibits more negative $\delta^{13}\text{C}_{\text{DIC}}$ (and $\delta^{13}\text{C}_{\text{carb}}$), slightly closer to OC signatures, whereas the $\delta^{13}\text{C}_{\text{DIC}}$ of the
384 three SOB lakes lie very far from OC isotopic signatures (Fig. 4). Dense vegetation surrounds La Alberca (Fig. S1),
385 making it the only lake in this study where OC respiration could be a significant source of inorganic C to the water
386 column (potentially influencing the P_{CO_2} , [DIC] and pH profiles described above).

387 In summary, a combination of very local and external environmental factors generates the contrasting water
388 chemistries of the lakes, notably a gradient in their alkalinity/[DIC]. This chemical variability stems from the exact
389 nature of the basement rocks, the distinct groundwater flow paths feeding the lakes, differences in evaporation
390 rates, and potentially different volcanic- CO_2 degassing regimes.

391

392 **5.1.2 Influence of alkalinity on physico-chemical stratification in the four lakes**

393 Stratified water columns can sustain strong physico-chemical gradients, where a wide range of biogeochemical
394 reactions impacting the C cycle can take place (e.g. Jézéquel et al., 2016). In the four lakes studied here, the
395 evolution of pH with depth exemplifies the interplay between the alkalinity gradient, the physico-chemical
396 stratification of the lakes, and their respective C cycle. The pH shows a stratified profile in La Alberca and La
397 Preciosa, but remains constant in Atexcac and Alchichica. The decline in pH at the oxycline of La Preciosa is
398 associated with the decrease in POC and chlorophyll a concentrations and $\delta^{13}\text{C}_{\text{DIC}}$ values, reflecting the impact of
399 oxygen respiration (i.e. carbon remineralization) at this depth (Figs. 2-4). In La Alberca, the surface waters are
400 markedly more alkaline than the bottom waters, with a two-step decrease in pH occurring at 8 m and 17 m (with a
401 total drop of 1.5 pH unit). As in La Preciosa, this pH decrease likely results from high OM respiration, although
402 input of volcanic acidic gases (e.g. dissolved CO_2 with $\delta^{13}\text{C} \sim -5 \text{‰}$) might also contribute to the pH decrease in
403 the bottom waters, reflected by negative $\delta^{13}\text{C}_{\text{DIC}}$ signatures and an increase of [DIC] and conductivity in the
404 hypolimnion (Figs. 2 and 4). By contrast, while the same evidence for oxygen respiration ([POC], chlorophyll a)
405 can be detected in the other two lakes, it does not impact their pH profile in a similar way (Fig. 2). This result
406 suggests that the acidity generated by OM respiration (and possibly volcanic- CO_2 degassing) is buffered by the
407 much higher alkalinity measured in these two lakes.

408 External forcings such as lake hydrology and fluid sources thus impact the alkalinity buffering capacity of these
409 lakes and influence the vertical pH profile of the water columns, which is particularly important considering the
410 critical interplay between pH and biogeochemical reactions affecting the C cycle (e.g. Soetaert et al., 2007).

411

412 **5.1.3 Sinks of DIC along the alkalinity gradient**

413 Interplay between pH and sources of alkalinity/DIC in the lakes also has a strong impact on their C storage capacity
414 as it can result in different fluxes of the C sinks (inorganic and organic C precipitation / sedimentation, CO_2
415 degassing).

416 Alkaline pH can store large quantities of DIC because it favors the presence of HCO_3^- and CO_3^{2-} species over
417 H_2CO_3^* (the intermediate species between gaseous $\text{CO}_{2(\text{g})}$ and bi-/carbonate ions, defined here as the sum of H_2CO_3
418 and $\text{CO}_{2(\text{aq})}$). Carbonate and bicarbonate ions represent over 99% of total DIC in the four lakes (Table S2). In La

419 Alberca de los Espinos, the lake with the lowest DIC, the surface water $p\text{CO}_2$ is slightly lower than atmospheric
420 $p\text{CO}_{2\text{atm}}$ (Table S2). By contrast, large amounts of CO_2 degas at the surface of the SOB lakes, as indicated by their
421 elevated surface water $p\text{CO}_2$, from 2 to 5 times higher than atmospheric $p\text{CO}_{2\text{atm}}$ (Table S2). These different CO_2
422 degassing potentials are consistent with the notion that higher DIC concentrations favor CO_2 degassing through
423 higher $p\text{CO}_2$ (e.g. Duarte et al., 2008). Although La Alberca and Alchichica (the two endmembers of the alkalinity
424 gradient) have the same surface water pH, CO_2 degassing is three times higher at Alchichica, for a given value of
425 gas transfer velocity.

426 Another important C sink for these lakes is the precipitation of carbonate minerals, found in the microbialites and
427 lake sediments. Lake alkalinity and resulting mineral saturation index greatly influence the amount of C
428 precipitated from the lake waters. Although the four lakes are supersaturated with aragonite, calcite and the
429 precursor phase monohydrocalcite, they present highly contrasted amounts of carbonate deposits (Zeyen et al.,
430 2021). The occurrence of microbialites increases along the alkalinity gradient, with limited presence at La Alberca,
431 and more massive deposits at Atexcac and Alchichica (Zeyen et al., 2021; Fig. S1). Similarly, surficial sediments
432 contain only 16 wt. % for La Alberca, but from 40 to 62 wt. % carbonates for the SOB lakes (Table S3). Thus, the
433 SOB lakes seem to bury more C than La Alberca de los Espinos. Nonetheless, the data from May 2019 indicate
434 that La Alberca was the only one of the four lakes with a $p\text{CO}_2$ slightly lower than atmospheric $p\text{CO}_{2\text{atm}}$, thus
435 representing a net sink of C. Classifying the three other lakes as net C sources or sinks – notably in order to see
436 the influence of their respective position in the alkalinity gradient – will require a more detailed description of C
437 in- and out-fluxes since they all store and emit significant amounts of C (as organic and inorganic C deposits and
438 via CO_2 degassing, respectively). However, such a C budget is out of the scope of the present study.

439

440 **5.1.4 Isotopic signatures of inorganic C in the four lakes ($\delta^{13}\text{C}_{\text{DIC}}$ and $\delta^{13}\text{C}_{\text{Carbonates}}$)**

441 The DIC isotopic composition of the lakes (between ~ -3 and $+2$ ‰ on average; Table S1) is consistent with the
442 DIC sources described above. The lower $\delta^{13}\text{C}_{\text{DIC}}$ in La Alberca is consistent with influence of remineralized OC
443 and/or volcanic CO_2 . The $\delta^{13}\text{C}_{\text{DIC}}$ in the SOB lakes suggests groundwater $\delta^{13}\text{C}_{\text{DIC}}$ values resulting from the
444 dissolution of the Cretaceous limestone basement.

445 By controlling DIC speciation ($\text{H}_2\text{CO}_3/\text{CO}_{2(\text{aq})}$, HCO_3^- , CO_3^{2-}), pH also strongly influences $\delta^{13}\text{C}_{\text{DIC}}$. Indeed, there
446 is a temperature-dependent fractionation of up to 10 ‰ between the different DIC species (Emrich et al., 1970;
447 Mook et al., 1974; Bade et al., 2004; Table S6). The Mexican lakes present $\delta^{13}\text{C}_{\text{DIC}}$ values that are common for
448 lakes with a pH around 9 (Bade et al., 2004), where DIC is dominated by HCO_3^- . However, the pH values of the
449 four lakes studied here are too similar to explain the significant difference between their $\delta^{13}\text{C}_{\text{DIC}}$ (Fig. 4; $p=4.2 \times 10^{-3}$
450 for La Preciosa and Atexcac, which have the closest $\delta^{13}\text{C}_{\text{DIC}}$). Part of the variability of $\delta^{13}\text{C}_{\text{DIC}}$ among the lakes
451 may result from their distinct evaporation stages, as the mean $\delta^{13}\text{C}_{\text{DIC}}$ values of the lakes broadly correlate with
452 their salinity/alkalinity (Fig. S3b). Evaporation generally increases the $\delta^{13}\text{C}_{\text{DIC}}$ of residual waters by increasing
453 lake $p\text{CO}_2$ and primary productivity, which bolsters CO_2 degassing and organic C burial, both having low $\delta^{13}\text{C}$
454 compared to DIC (e.g. Li and Ku, 1997; Talbot, 1990). Accordingly, the $p\text{CO}_2$ of La Alberca is lower than that of
455 the other lakes (Table S2). The $\delta^{13}\text{C}_{\text{DIC}}$ in lakes with lower DIC concentrations is expected to be more easily
456 influenced by exchanges with other carbon reservoirs, such as organic carbon (through photosynthesis/respiration),

457 or other DIC sources (e.g., depleted volcanic CO₂ or groundwater DIC), compared with buffered, high DIC lakes
 458 (Li and Ku, 1997). As a result, the low DIC/alkalinity concentration in La Alberca features the lowest δ¹³C_{DIC} of
 459 the four lakes, likely reflecting organic and/or volcanic C influence and thus higher responsiveness to
 460 biogeochemical processes of the inorganic C reservoir. By contrast, the three SOB lakes exhibit δ¹³C_{DIC} with less
 461 internal variability, with a maximum amplitude of 0.7 ‰ within a single water column.

462 Surficial sedimentary carbonates are in isotopic equilibrium with the δ¹³C_{DIC} of the water columns, within the
 463 uncertainty of δ¹³C_{DIC} measurement, and more specifically with the δ¹³C_{DIC} values at the oxycline/thermocline of
 464 the lakes (Tables S6 and S7). The δ¹³C_{DIC} at equilibrium with carbonates is estimated by correcting the carbonates
 465 C isotope composition (δ¹³C_{carb}) by the fractionation value between DIC and the different carbonate mineralogies
 466 (supplementary text S2). Therefore, the δ¹³C_{carb} also follows and reflects the alkalinity gradient, with the lowest
 467 δ¹³C_{carb} found in the surficial sediments of La Alberca (~ -1.5 ‰), intermediate values in La Preciosa and Atecac
 468 (~ -2.5 ‰), and the highest values in Alchichica (~ +4.6 ‰) (Table S3).

469
 470 In summary, although all four lakes present the same general structure and environmental conditions (i.e. tropical
 471 alkaline stratified crater lakes), external and local factors (e.g. hydrology, fluid sources, and stratification
 472 characteristics) result in contrasting water chemistry compositions, which have a critical impact on the physico-
 473 chemical depth profiles of each lake and their biogeochemical carbon cycle functioning. These external factors
 474 represent a first-order control on the size, isotopic composition, and responsiveness to biogeochemical processes
 475 of the inorganic C reservoir. Lakes with the highest alkalinity/DIC content will poorly record internal biological
 476 processes. Interestingly, C storage in mineral carbonates seems to be significant in watersheds where carbonate
 477 deposits pre-exist in the geological substratum (here, the Cretaceous limestone basement), providing more alkaline
 478 and C-rich sources.

479

Symbols	Mathematical Expression	Signification
δ ¹³ C _X	$\left(\frac{\left(\frac{^{13}\text{C}}{^{12}\text{C}} \right)_X}{\left(\frac{^{13}\text{C}}{^{12}\text{C}} \right)_{VPDB}} - 1 \right) * 1000$	Relative difference in ¹³ C: ¹² C isotopic ratio between a sample of a given C reservoir and the international standard "Vienna Pee Dee Bee", expressed in permil (‰). δ ¹³ C _{total} represents the weighted average of δ ¹³ C for all DIC and POC.
Δ ¹³ C _{X-Y}	$= \delta^{13}\text{C}_X - \delta^{13}\text{C}_Y \approx 1000 \ln \alpha_{X-Y}$	Apparent isotopic fractionation between two reservoirs 'X' and 'Y'. Difference between their measured C isotope compositions approximating the fractionation α in ‰.
ε _{X-CO2}	$= (\alpha_{X-CO2} - 1)1000 \approx \delta^{13}\text{C}_X - \delta^{13}\text{C}_{CO2}$	Calculated isotopic fractionation between a reservoir 'X' and CO _{2(aq)} . α _{X-CO2} is calculated as (δ ¹³ C _X +1000)/(δ ¹³ C _{CO2} +1000) where δ ¹³ C _X is measured and δ ¹³ C _{CO2} is computed based on DIC isotopic composition and speciation (see supplementary text S3).

480

481 Table 2
482 Index for mathematical notations used in the text including C isotopic composition of a reservoir X ($\delta^{13}\text{C}_X$),
483 isotopic discrimination between the two carbon reservoirs X and Y ($\Delta^{13}\text{C}_{X-Y}$). In the main text, we report organic
484 C isotope discrimination *versus* both bulk DIC ($\Delta^{13}\text{C}_{\text{POC-DIC}}$) – in a way to facilitate studies intercomparison and
485 because it is the commonly reported raw measured data (Fry, 1996) – and calculated $\text{CO}_{2(\text{aq})}$ ($\epsilon_{\text{POC-CO}_2}$) in order to
486 discuss the intrinsic isotopic fractionations associated with the lakes metabolic diversity. All C isotope values and
487 fractionations are reported relative to the international standard VPDB (Vienna Pee Dee Belemnite).

488

489

490 **5.2. Particulate organic carbon: from water column primary production to respiration recycling and** 491 **sedimentary organic matter**

492 **5.2.1. Particulate organic C sources**

493 *Primary productivity by oxygenic photosynthesis in the upper water column*

494 The C:N ratios of water-column POM and bulk organic matter in the sediments of the four lakes ranged from 6 to
495 13 (Fig. 3), close to the phytoplankton Redfield but much lower than land plant ratios. Yet abundant vegetation
496 covers the crater walls of La Alberca and, to a lesser extent, of Atexcac, and some plant debris was found in the
497 sediment cores of these two lakes. Its analysis resulted in high C:N ratios (between 24 and 68), typical of plant
498 tissues and significantly higher than those of the bulk sediment and water column organic matter. Thus, the
499 allochthonous organic carbon in these two lakes does not significantly contribute to their bulk organic signal. All
500 four crater lakes are endorheic basins, with no surface water inflow or outflow, supporting the predominantly
501 autochthonous origin of organic carbon sources (Alcocer et al., 2014b), from planktonic autotrophic C fixation.

502 The importance of planktonic autotrophic C fixation as a major source of POC in the four lakes is further supported
503 by the assessment of the isotopic discrimination between DIC and organic biomass, expressed as $\Delta^{13}\text{C}_{\text{POC-DIC}}$ and
504 $\epsilon_{\text{POC-CO}_2}$ (Table 2). The $\Delta^{13}\text{C}_{\text{POC-DIC}}$ varies between ~ -29 and -23 ‰ (corresponding to $\epsilon_{\text{POC-CO}_2}$ between ~ -19 and
505 -13 ‰) throughout the four water columns, within the typical range of planktonic oxygenic phototrophs (Pardue
506 et al., 1976; Sirevag et al., 1977; Thomas et al., 2019). Yet these values exhibit variability – both within a single
507 water column (up to 4.5 ‰) and among the four lakes (up to 6 ‰, Figs. 4 and 5). The $\Delta^{13}\text{C}_{\text{POC-DIC}}$ variability may
508 reflect several abiotic and biotic factors.

509 Notably, lower DIC availability in La Alberca and La Preciosa probably makes the carboxylation step less limiting
510 during photosynthesis (e.g. O'Leary, 1988; Descolas-Gros and Fontungne, 1990; Fry, 1996), decreasing $|\epsilon_{\text{POC-CO}_2}|$
511 in these lakes (between 14.5 and 17.7 ‰ at the peak of Chl. a) compared with Atexcac and Alchichica (Fig. 5a;
512 between 17.5 and 19.2 ‰). Lower $\text{CO}_{2(\text{aq})}$ availability and/or higher reaction rates result in transport-limited rather
513 than carboxylation-limited fixation, with smaller C isotope fractionation between POC and DIC (Pardue et al.,
514 1976; Zohary et al., 1994; Fry, 1996; Close and Henderson, 2020). The isotopic fractionation associated with
515 diffusion is much smaller than with carboxylation, and a higher proportion of the DIC entering the cells is
516 converted into organic biomass (e.g. Fogel and Cifuentes, 1993). We consistently notice a correlation among the
517 lakes between $\alpha(\text{CO}_{2(\text{aq})})$ (or [DIC]) and $|\epsilon_{\text{POC-CO}_2}|$ at depths where oxygenic photosynthetic peaks (Fig. 6).

518 Furthermore, La Alberca and La Preciosa are considered less oligotrophic than the two other lakes (Lugo et al.,
 519 1993; Vilaclara et al., 1993; Havas et al., submitted), with higher chlorophyll a contents and thus smaller $|\epsilon_{\text{POC-CO}_2}|$
 520 (Fig. 5). Higher water temperatures in La Alberca de los Espinos (by ~ 3 °C) could also partly contribute to a
 521 smaller $|\epsilon_{\text{POC-CO}_2}|$ in this lake (Sackett et al., 1965; Pardue et al., 1976; Descolas-Gros and Fontungne, 1990).

522 Unlike $\delta^{13}\text{C}_{\text{DIC}}$, organic carbon isotope signatures do not evolve linearly with the alkalinity/salinity gradient,
 523 suggesting other lake- and microbial-specific controls on these signatures. These controls include: diffusive or
 524 active uptake mechanisms, specific carbon fixation pathways, the fraction of intracellular inorganic carbon
 525 released out of the cells, cell size and geometry (Werne and Hollander, 2004 and references therein) and
 526 remineralization efficiency. Moreover, an increasing amount of isotopic data has evidenced a significant variability
 527 of the isotopic fractionation achieved by different purified RuBisCO enzymes ($\epsilon_{\text{RuBisCO}}$, Iñiguez et al., 2020), and
 528 even by a single RuBisCO form (Thomas et al., 2019). Thus, caution should be paid to the interpretation of the
 529 origin of small isotopic variations of the biomass in distinct environmental contexts because RuBisCO alone can
 530 be an important source of this variability (Thomas et al., 2019).

531

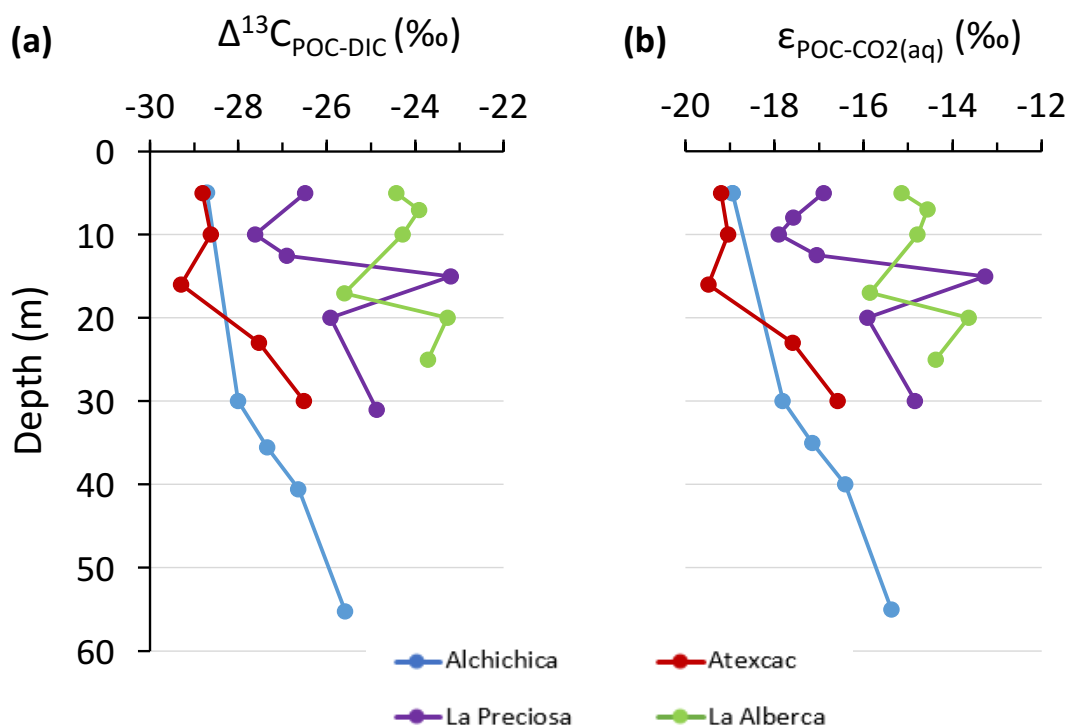


Figure 5. Isotopic fractionations between POC and DIC in the water columns of the four lakes, expressed as a) $\Delta^{13}\text{C}_{\text{x-y}}$ and b) $\epsilon_{\text{POC-CO}_2}$. Refer to Table 2 for more detail about the Δ and ϵ notations.

532 *Primary production in the anoxic hypolimnion*

533 Anoxygenic autotrophs commonly thrive in anoxic
 534 bottom waters of stratified water bodies (e.g.
 535 Pimenov et al., 2008; Zyakun et al., 2009; Posth et
 536 al., 2017; Fulton et al., 2018; Havig et al., 2018).
 537 They have been identified at different depths in the
 538 four Mexican lakes (Macek et al., 2020; Iniesto et al.,
 539 2022). In our samples collected during the
 540 stratification period, anoxygenic autotrophs appear to
 541 have a distinct impact on the C cycle of La Alberca
 542 and Atexcac only. Lake Atexcac records a
 543 concomitant decrease in [DIC] and increase in
 544 $\delta^{13}\text{C}_{\text{DIC}}$ in the anoxic hypolimnion at 23 m, below the
 545 peak of Chl a, suggesting autotrophic C fixation by
 546 chemoautotrophy or anoxygenic photosynthesis. The
 547 calculated $\epsilon_{\text{POC-CO}_2}$ at 23 m (-17.3 ‰) is consistent
 548 with C isotope fractionation by purple- and green-
 549 sulfur-anoxygenic bacteria (PSB and GSB), while
 550 $\epsilon_{\text{POC-CO}_2}$ in La Alberca's hypolimnion (~ -15 ‰) is
 551 closer to GSB canonical signatures (Posth et al., 2017
 552 and references therein) (Fig. 5b). In La Alberca,
 553 anoxygenic primary productivity is suggested by
 554 increasing POC concentrations below the oxycline,
 555 showing a distinct isotopic signature (Figs. 4 and 5).
 556 We also observe a Chl a peak in the anoxic
 557 hypolimnion of this lake (Fig. 2), which likely
 558 represents a bias of the probe towards some
 559 bacteriochlorophyll pigments typical of GSB (see
 560 supplementary text S4). In Atexcac, C fixation by
 561 anoxygenic autotrophs at 23 m causes a shift in the DIC
 562 reservoir, while oxygenic photosynthesis at 16 m does
 563 not, suggesting that anaerobic autotrophs are the main
 564 autotrophic metabolisms in this lake (in terms of DIC
 565 uptake). In La Alberca, the increase in [POC] to
 566 maximum values below the oxycline also supports the
 567 predominance of anoxygenic *versus* oxygenic
 568 autotrophy (Fig. 3), similarly to other stratified water
 569 bodies exhibiting primary production clearly dominated
 570 by anoxygenic metabolisms (Fulton et al., 2018).

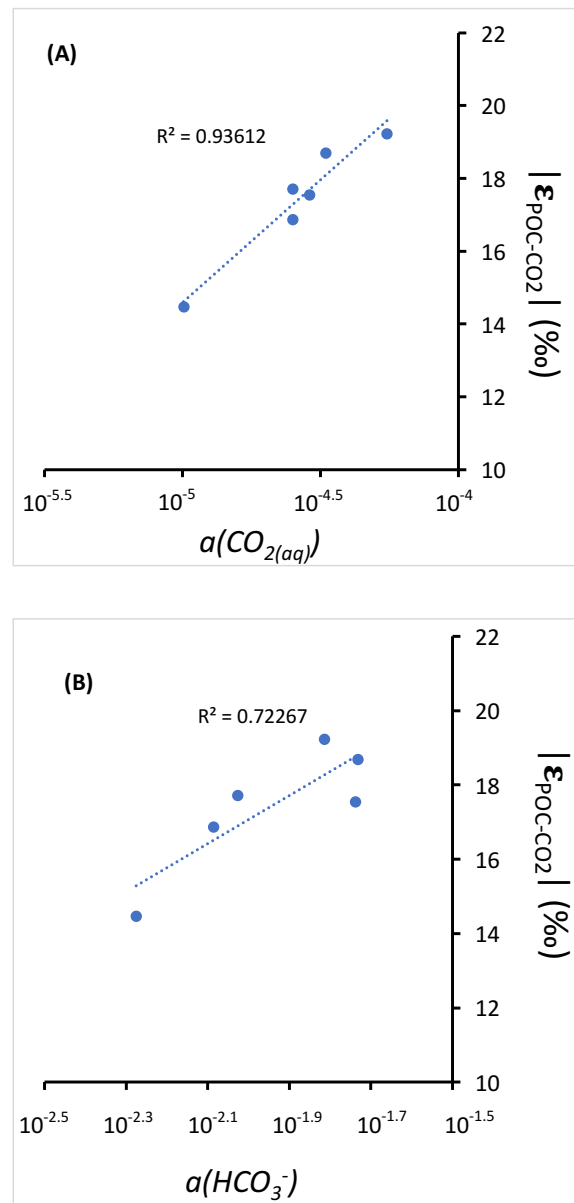


Figure 6.

Cross plots of DIC species activities *versus* absolute values of calculated C isotopic fractionations between POC and CO_2 at depths of peak oxygenic photosynthesis where data was available (5 and 30 m for Alchichica, 16 m for Atexcac, 10 and 12.5 m for La Preciosa and 7 m for La Alberca). (A) Dissolved $\text{CO}_{2(\text{aq})}$ activity and (B) bicarbonate activity as functions of $|\epsilon_{\text{POC-CO}_2}|$ in ‰ plus linear correlation trends and corresponding R^2 .

571 Lastly, at 23 m in Atexcac and 17 m in La Alberca, we find a striking turbidity peak precisely where the redox
572 potential and the concentration of dissolved Mn drops (Fig. 2). In Atexcac, the concentration in dissolved metals
573 such as Cu, Pb, or Co also drops at 23 m (Fig. S4). In La Alberca, a peak of particulate Mn concentration is detected
574 at 15 m (Fig. 2; data unavailable for Atexcac). This peak is most likely explained by the precipitation of Mn mineral
575 particles, where reduced bottom waters meet oxidative conditions prevailing in the upper waters. These oxidized
576 Mn phases can be used as electron acceptors during chemoautotrophy (Havig et al., 2015; Knossow et al., 2015;
577 Henkel et al., 2019; van Vliet et al., 2021). Even at a low particle density, such phases can catalyze abiotic oxidation
578 of sulfide to sulfur compounds, which in turn can be used and further oxidized to sulfate by phototrophic or
579 chemoautotrophic sulfur-oxidizing bacteria (van Vliet et al., 2021). Autotrophic sulfur oxidation is also consistent
580 with the small increase in $[\text{SO}_4^{2-}]$ observed at 23 m in Atexcac (Table S4).

581 In summary, combined POC and DIC data allowed us to recognize the most representative autotrophic
582 metabolisms in the Mexican lakes. The upper water columns are all dominated by oxygenic photosynthesis. Lower
583 in the water columns, anoxygenic photosynthesis and/or chemoautotrophy were found to have a noticeable impact
584 on POC and DIC reservoirs in La Alberca and Atexcac only. Their activity was associated with metal elements
585 cycling. More specifically in La Alberca, the anoxygenic phototrophs correspond to GSB.

586

587

588 **5.2.2. Sinks of particulate organic carbon: respiration and sedimentation**

589 *Aerobic respiration at the oxycline*

590 At the oxycline of stratified water bodies, aerobic respiration of OM by heterotrophic organisms favors the
591 transition from oxygenated upper layers to anoxic bottom waters. In the water column of the four lakes, $\Delta^{13}\text{C}_{\text{POC-DIC}}$
592 (and $\varepsilon_{\text{POC-CO}_2}$) show increasing values in the hypolimnion, and especially below the chlorophyll a peaks (Figs. 2
593 and 5). The $\Delta^{13}\text{C}_{\text{POC-DIC}}$ trend correlates with increasing $\delta^{13}\text{C}_{\text{POC}}$, decreasing $(\text{C:N})_{\text{POM}}$ ratios as well as decreasing
594 POC concentrations except in La Alberca (Figs. 3 and 4). Decreasing POC concentrations near the oxycline and
595 redoxcline are consistent with the fact that part of the upper primary production is degraded deeper in the water
596 columns and/or that there is less primary production in the anoxic bottom waters. Increased $\delta^{13}\text{C}_{\text{POC}}$ in the
597 hypolimnion of the lakes is consistent with heterotrophic activity and points out that POC at these depths could
598 mainly record secondary production rather than being a residue of sinking degraded OM formed by primary
599 production. Heterotrophic bacteria preferentially grow on available ^{13}C -enriched amino acids and sugars, thus
600 becoming more enriched than their C source (Williams and Gordon, 1970; Hayes et al., 1989; Zohary et al., 1994;
601 Briones et al., 1998; Lehmann et al., 2002; Jiao et al., 2010; Close and Henderson, 2020). The decrease in C:N
602 ratios in the POM also reinforces this conclusion since secondary heterotrophic bacteria biomass generally have
603 C:N between 4 and 5 (Lehmann et al., 2002), whereas residual degraded OM from primary producers would carry
604 higher C:N signatures (van Mooy et al., 2002; Buchan et al., 2014). These latter signatures are not recorded by
605 POM in the lower water columns of the lakes (Fig. 3).

606 The $\delta^{13}\text{C}_{\text{DIC}}$ signatures in La Preciosa and Alchichica are consistent with the mineralization of OM as they exhibit
607 lower values below the oxycline than in surficial waters (Figs. 2 and 4). Similarly to what is observed in several
608 other water bodies and notably stratified water columns such as the Black Sea (e.g. Fry et al., 1991), surface

609 photosynthesis increases $\delta^{13}\text{C}_{\text{DIC}}$ by fixing light DIC, while respiration transfers light OC back to the DIC pool at
610 depth. Such a decrease in $\delta^{13}\text{C}_{\text{DIC}}$ can also be seen in the oxycline of Lake La Alberca between 7 and 10 m.

611
612 *Influence of methanogenesis in Lake La Alberca de los Espinos*

613 La Alberca shows the least saline/alkaline water column and most peculiar geochemical depth profiles among the
614 four lakes. Notably, its [DIC] and $\delta^{13}\text{C}_{\text{DIC}}$ (the lowest of the studied lakes) increase from the lower metalimnion to
615 the hypolimnion, and further into the first cm of sediment porewaters, with $\delta^{13}\text{C}_{\text{DIC}}$ reaching almost 10 ‰ (Figs. 3;
616 4). The calculated CO_2 partial pressure (P_{CO_2}) increases downward from slightly less than $1 \times P_{\text{CO}_2\text{-atm}}$ near the lake
617 surface up to almost 40x at the bottom of the lake (Table S2).

618 While the increase of [POC] at depth may contribute to the observed $\delta^{13}\text{C}_{\text{DIC}}$ increase, by mass balance, it should
619 also lower the [DIC] instead of increasing it. Similarly, the sinking of POC at depth followed by its
620 remineralization into DIC cannot explain the $\delta^{13}\text{C}_{\text{DIC}}$ trend since it would lower the $\delta^{13}\text{C}_{\text{DIC}}$ in the hypolimnion
621 (Fig. 4). Overall, these observations require that a significant source of inorganic ^{13}C -rich carbon fuels the bottom
622 waters of La Alberca de los Espinos. The source of heavy carbon most likely results from methanogenesis, which
623 consumes organic carbon in the sediments and produces ^{13}C -depleted methane and ^{13}C -rich carbon dioxide
624 diffusing upward in the water column (i.e. acetoclastic methanogenesis, dominant in lacustrine contexts, Whiticar
625 et al., 1986). Methanogenesis, as an “alternative” OM remineralization pathway would be favored in La Alberca,
626 because it is relatively rich in OM (notably with high [DOC], Havas et al., submitted), and depleted in SO_4^{2-}
627 (Wittkop et al., 2014; Birgel et al., 2015; Cadeau et al., 2020) compared with the three other Mexican lakes. Based
628 on the $\delta^{13}\text{C}_{\text{SOC}}$ and porewater $\delta^{13}\text{C}_{\text{DIC}}$, we can tentatively calculate the methane isotopic signature in La Alberca
629 (see supplementary text S5). The resulting $\delta^{13}\text{C}_{\text{CH}_4}$ in the first 10 cm of sediments is between -59 and -57 ‰, which
630 is consistent with the range of isotopic composition of methane after biogenic methanogenesis (Whiticar et al.,
631 1986).

632 Upward diffusing methane may be either (i) partly lost from the lake’s surface (i.e. escaping the system) by
633 degassing or (ii) totally retained in the water column by complete oxidation (either abiotically by oxygenated
634 surface waters or biologically by methanotrophic organisms). The oxidation of CH_4 in the water column should
635 lead to the formation of ^{13}C -depleted carbon dioxide that would mix back with the lake DIC (and notably with
636 heavy methanogenic CO_2 produced at depth) and/or ^{13}C -depleted biomass (as POC or SOC) if it occurs through
637 methanotrophy. Thus, the net effect of combined methanogenesis and methane oxidation is expected to (i) generate
638 a $\delta^{13}\text{C}_{\text{DIC}}$ gradient from high to low values between the sediment porewaters and the oxycline as proposed
639 elsewhere (Assayag et al., 2008; Wittkop et al., 2014) and (ii) progressively lower sedimentary $\delta^{13}\text{C}_{\text{SOC}}$ in the case
640 of methanotrophy. Abiotic oxidation of methane by dioxygen is consistent with the observation that $\delta^{13}\text{C}_{\text{DIC}}$
641 decreases from porewaters ($\sim +10$ ‰) to the oxycline (-4 ‰), reaching minimum values where dissolved- O_2 starts
642 to appear (Fig. 2). Microbial anaerobic oxidation of methane (AOM) could occur at the 17 m depth through Mn-
643 oxide reduction (Cai et al., 2021; Cheng et al., 2021) and possibly bacterial sulfate-reduction closer to the water-
644 sediment interface, as inferred for the surficial sediments of meromictic Lake Cadagno (Posth et al., 2017). Indeed,
645 we observe a net increase of particulate Fe and S concentrations at a depth of 25 m and a peak of solid sulfide
646 minerals in the surficial sediments (Fig. S5). However, $\delta^{13}\text{C}_{\text{SOC}}$ and $\delta^{13}\text{C}_{\text{POC}}$ are far from calculated $\delta^{13}\text{C}_{\text{CH}_4}$,

647 suggesting that AOM is not a major process in the bottom lake waters and surface sediments (Lehmann et al.,
648 2004) and thus that methanotrophy is not the main CH₄ oxidation pathway in Lake La Alberca.

649 Alternatively, if some portion of the methane escaped oxidation and degassed out of the lake, $\delta^{13}\text{C}_{\text{DIC}}$ would likely
650 be driven to extreme positive values with time (Gu et al., 2004; Hassan, 2014; Birgel et al., 2015; Cadeau et al.,
651 2020). Methane escape is not consistent with the average $\delta^{13}\text{C}_{\text{DIC}}$ in La Alberca (~ -3 ‰; Fig. 4), unless an
652 additional counterbalancing source of DIC to this lake exists. This source of DIC could be volcanic CO₂-degassing
653 (see section 5.1.1). Such a contribution may maintain the lake's average $\delta^{13}\text{C}_{\text{total}}$ close to a mantle isotopic signature
654 and notably away from extreme positive values if CH₄-escape dominated. It is also possible that volcanic CO₂
655 degassing is coupled to methanogenesis by CO₂ reduction in addition to the acetoclastic type described above.

656 Although volcanic CO₂ could be an important source in the C mass balance of Lake La Alberca, we note that it
657 cannot explain the very positive $\delta^{13}\text{C}_{\text{DIC}}$ in the sediment porewaters alone, thus bolstering the identification of
658 methanogenesis. Importantly, this methane cycle is cryptic to the sediment record, as it is evidenced in the
659 dissolved inorganic C phase, but not in the sedimentary organic matter or carbonates. This is a consequence of the
660 lake's stratified nature, where the location of carbonate precipitation and methane production is decoupled.

661

662 *Transfer of OM from the water column to the surficial sediments*

663 The OC content in the first 12 cm of the sediment cores from the four lakes ranges from 1 to 13 wt. % (Table S3).
664 These concentrations are relatively elevated considering the predominantly autochthonous nature of OC and the
665 oligotrophic conditions in these lakes (Alcocer et al., 2014; Havas et al., submitted). In Lake Alchichica, the recent
666 OC burial flux in the sediment was estimated to represent between 15 and 26 g.yr⁻¹.m⁻² (Alcocer et al., 2014).
667 These values are within the range observed for small lakes around the world (Mulholland and Elwood, 1982; Dean
668 and Gorham, 1998; Mendonça et al., 2017), though most of them receive allochthonous OM inputs. Different
669 factors can favor the preservation of OM including lower respiration and oxidation rates due to anoxic bottom
670 waters and scarce benthic biota and/or high sedimentation rates (Alcocer et al., 2014). Anaerobic respiration clearly
671 occurs in the four lakes to some extent, as detailed for La Alberca, and as seen in the surficial sediment data of the
672 other lakes as well (decreasing $\delta^{13}\text{C}_{\text{DIC}}$ in Alchichica, increasing C:N ratio in Atexcac and La Preciosa; Table S3).
673 Nonetheless, the anoxic conditions prevailing in the hypolimnion most of the year are significantly more favorable
674 to OM preservation than oxic conditions (Sobek et al., 2009; Kuntz et al., 2015). While the yearly mixing oxidizes
675 most of the water column during the winter, it also generates a bloom of diatoms which fosters OM production
676 (through shuttling up of bio essential nutrient such as N and Si) and development of anoxia (e.g. Adame et al.,
677 2008). In Alchichica, the large size of some of the phytoplankton was also suggested to favor OM preservation
678 (Adame et al., 2008; Ardiles et al., 2011). Because bacterial sulfate reduction (BSR) is a major remineralization
679 pathway in SO₄-rich environments (e.g. Jørgensen, 1982), the low sulfate content in La Alberca probably favors
680 the preservation of high TOC in the sediments. Even though, appreciable BSR rates may occur in this lake (see
681 discussion above and Fig. S5), similarly to other sulfate-poor environments due to rapid S-cycling (e.g. Vuillemin
682 et al., 2016; Friese et al., 2021). Again, a complete mass-balance of these lakes C fluxes will be required to estimate
683 their net C emission or sequestration behavior.

684 Although the nature and geochemical signatures of the OM that deposits in the sediments may vary throughout the
685 year, it is interesting to infer from what part(s) of the water column surficial sedimentary OM comes during the
686 stratified seasons. In the three lakes from the SOB, $\delta^{13}\text{C}_{\text{SOC}}$ and $(\text{C:N})_{\text{SOM}}$ signatures of the surficial sedimentary
687 OM lie somewhere between POM signatures from the upper water column and from the hypolimnion (Figs. 3, 4).
688 More precisely, in Alchichica, the most surficial $\delta^{13}\text{C}_{\text{SOC}}$ and $(\text{C:N})_{\text{SOM}}$ signatures (-25.7 ‰ and 10.4, respectively)
689 are much closer to values recorded in the upper water column (~ -26.5 ‰ and 10.5, respectively), implying that
690 the upper oxygenic photosynthesis production is primarily recorded. It is consistent with previous studies
691 suggesting that most of the phytoplankton biomass being exported is composed of diatoms (Ardiles et al., 2011).
692 In Lake Atexcac, however, $\delta^{13}\text{C}_{\text{SOC}}$ and $(\text{C:N})_{\text{SOM}}$ signatures (~ -26.8 ‰ and 8, respectively) are closer to values
693 recorded in the hypolimnion (~ -26.5 ‰ and 6.5, respectively) suggesting that SOM records mostly the anaerobic
694 primary production.

695 In La Alberca, surficial $\delta^{13}\text{C}_{\text{SOC}}$ is markedly more negative (by ~ 2 to 3 ‰) than the deepest and shallowest water
696 column values (Fig. 4), but close to what is recorded at the redoxcline depth of 17 m. However, the $(\text{C:N})_{\text{SOM}}$
697 values are much higher than what is measured anywhere in the water column, which is consistent with OM
698 remineralization by sulfate-reduction and methanogenesis in the sediments of this lake. Therefore, OM
699 biogeochemical signatures in the surficial sediments of La Alberca could be strongly influenced by early diagenesis
700 occurring at the water-sediment interface – despite favorable conditions for OM preservation.

701 In summary, the OM depositing at the bottom of these stratified lakes does not always record geochemical
702 signatures from the same layers of the water columns and can be modified by very early diagenesis. It does not
703 necessarily record the signatures of primary production by oxygenic photosynthesis from the upper column. For
704 example, in Lake Atexcac, sedimentary OM records primary production by anoxygenic photosynthesis, even
705 though POC concentration is highest in the upper water column. This result highlights the diversity of geochemical
706 signatures that can stem from continental environments despite their geographical, geological, and climatic
707 proximity. A deeper understanding of the OM transfer process from water column to sediment will require more
708 detailed analyses and comparison of the different OM pigments and molecules and could have strong implications
709 for the interpretation of the fossil record in deep anoxic time.

710

711 6. CONCLUSIONS AND SUMMARY

712 The carbon cycles of four stratified alkaline crater lakes were described and compared based on the concentration
713 and isotopic compositions of DIC and POC in the water columns and surficial (~10 cm) sedimentary carbonates
714 and organic carbon. Overall our study shows the wide diversity of geochemical signatures found in continental
715 stratified environments despite similar geological and climatic contexts. We identify different regimes of C cycling
716 in the four lakes due to different biogeochemical reactions related to slight environmental and ecological
717 variations. In more detail, we show that:

718 - External abiotic factors, such as the hydrological regime and the inorganic C sources in the lakes, control
719 their alkalinity and thus, the buffering capacity of their waters. In turn, these differences in buffering
720 capacity constrain variations in pH along the stratified water columns as well as the inorganic C isotope
721 signatures recorded in the water columns and sediments of the lakes. The $\delta^{13}\text{C}_{\text{carb}}$ reflects the abiotic

722 factors generating the alkalinity gradient, but it is poorly representative of biological processes in lakes
723 with high alkalinity. The external environmental factors further impact the C mass balance of the lakes
724 with probable consequences on their net C-emitting or -sequestering status.

725 - Based on POC and DIC concentrations and isotopic compositions, combined with physico-chemical
726 parameters, we are able to identify the activity of oxygenic photosynthesis and aerobic respiration in the
727 four lakes studied. Anoxygenic photosynthesis and/or chemoautotrophy are also evidenced in two of the
728 lakes, but their POC and DIC signatures can be equivocal.

729 - Methanogenesis is evidenced in the surficial sediments of the OM-rich Lake La Alberca de los Espinos
730 and influences the geochemical signatures lower in the water column. However, it is recorded only in
731 analyses of porewater dissolved species, but not imprinted in the sedimentary archives (OM and
732 carbonates).

733 - The SOM geochemical signatures of these stratified lakes do not all record the same “biogeochemical
734 layers” of the water column (e.g. anaerobic vs. aerobic metabolisms), and, in some cases, can be greatly
735 modified by early diagenesis.

736

737 **Data Availability**

738 Data are publicly accessible at: <https://doi.org/10.26022/IEDA/112923>.

739

740 **Author Contributions**

741 RH and CT designed the study in a project directed by PLG, KB and CT. CT, MI, DJ, DM, RT, PLG and KB
742 collected the samples on the field. RH carried out the measurements for C data; DJ the physico-chemical parameter
743 probe measurements and EM provided data for trace and major elements. RH and CT analyzed the data. RH wrote
744 the manuscript with important contributions of all co-authors.

745

746 **Competing Interests**

747 The authors declare that they have no conflict of interest.

748

749 **Disclaimer**

750

751 **Acknowledgements**

752 This work was supported by Agence Nationale de la Recherche (France; ANR Microbialites, grant number ANR-
753 18-CE02-0013-02). The authors thank Anne-Lise Santoni, Elodie Cognard, Théophile Cocquerez and the GISMO
754 platform (Biogéosciences, Université Bourgogne Franche-Comté, UMR CNRS 6282, France). We thank Céline
755 Liorzou and Bleuenn Guéguen for the analyses at the Pôle Spectrométrie Océan (Laboratoire Géo-Océan, Brest,
756 France) and Laure Cordier for ion chromatography analyses at IPGP (France). We thank Nelly Assayag and Pierre
757 Cadeau for their help on the AP 2003 at IPGP.

758

759 **References**

760 Adame, M.F., Alcocer, J., Escobar, E., 2008. Size-fractionated phytoplankton biomass and its
761 implications for the dynamics of an oligotrophic tropical lake. *Freshw. Biol.* 53, 22–31.
762 <https://doi.org/10.1111/j.1365-2427.2007.01864.x>

763 Ader, M., Macouin, M., Trindade, R.I.F., Hadrien, M.-H., Yang, Z., Sun, Z., Besse, J., 2009. A
764 multilayered water column in the Ediacaran Yangtze platform? Insights from carbonate and organic
765 matter paired $\delta^{13}\text{C}$. *Earth Planet. Sci. Lett.* 288, 213–227. <https://doi.org/10.1016/j.epsl.2009.09.024>

766 Aharon, P., 2005. Redox stratification and anoxia of the early Precambrian oceans: Implications for
767 carbon isotope excursions and oxidation events. *Precambrian Res.* S0301926805000355.
768 <https://doi.org/10.1016/j.precamres.2005.03.008>

769 Alcocer, J., 2021. *Lake Alchichica Limnology*, Springer Nature. ed.

770 Alcocer, J., Ruiz-Fernández, A.C., Escobar, E., Pérez-Bernal, L.H., Oseguera, L.A., Ardiles-Gloria, V.,
771 2014. Deposition, burial and sequestration of carbon in an oligotrophic, tropical lake. *J. Limnol.* 73.
772 <https://doi.org/10.4081/jlimnol.2014.783>

773 Anderson, N.John., Stedmon, C.A., 2007. The effect of evapoconcentration on dissolved organic
774 carbon concentration and quality in lakes of SW Greenland. *Freshw. Biol.* 52, 280–289.
775 <https://doi.org/10.1111/j.1365-2427.2006.01688.x>

776 Ardiles, V., Alcocer, J., Vilaclara, G., Oseguera, L.A., Velasco, L., 2012. Diatom fluxes in a tropical,
777 oligotrophic lake dominated by large-sized phytoplankton. *Hydrobiologia* 679, 77–90.
778 <https://doi.org/10.1007/s10750-011-0853-7>

779 Armienta, M.A., Vilaclara, G., De la Cruz-Reyna, S., Ramos, S., Cenicerros, N., Cruz, O., Aguayo, A.,
780 Arcega-Cabrera, F., 2008. Water chemistry of lakes related to active and inactive Mexican volcanoes.
781 *J. Volcanol. Geotherm. Res.* 178, 249–258. <https://doi.org/10.1016/j.jvolgeores.2008.06.019>

782 Armstrong-Altrin, J.S., Madhavaraju, J., Sial, A.N., Kasper-Zubillaga, J.J., Nagarajan, R., Flores-Castro,
783 K., Rodríguez, J.L., 2011. Petrography and stable isotope geochemistry of the cretaceous El Abra
784 Limestones (Actopan), Mexico: Implication on diagenesis. *J. Geol. Soc. India* 77, 349–359.
785 <https://doi.org/10.1007/s12594-011-0042-3>

786 Assayag, N., Jézéquel, D., Ader, M., Viollier, E., Michard, G., Prévot, F., Agrinier, P., 2008. Hydrological
787 budget, carbon sources and biogeochemical processes in Lac Pavin (France): Constraints from $\delta^{18}\text{O}$
788 of water and $\delta^{13}\text{C}$ of dissolved inorganic carbon. *Appl. Geochem.* 23, 2800–2816.
789 <https://doi.org/10.1016/j.apgeochem.2008.04.015>

790 Assayag, N., Rivé, K., Ader, M., Jézéquel, D., Agrinier, P., 2006. Improved method for isotopic and
791 quantitative analysis of dissolved inorganic carbon in natural water samples. *Rapid Commun. Mass*
792 *Spectrom.* 20, 2243–2251. <https://doi.org/10.1002/rcm.2585>

793 Bade, D.L., Carpenter, S.R., Cole, J.J., Hanson, P.C., Hesslein, R.H., 2004. Controls of $\delta^{13}\text{C}$ -DIC in lakes:
794 Geochemistry, lake metabolism, and morphometry. *Limnol. Oceanogr.* 49, 1160–1172.
795 <https://doi.org/10.4319/lo.2004.49.4.1160>

796 Bekker, A., Holmden, C., Beukes, N.J., Kenig, F., Eglinton, B., Patterson, W.P., 2008. Fractionation
797 between inorganic and organic carbon during the Lomagundi (2.22–2.1 Ga) carbon isotope excursion.
798 *Earth Planet. Sci. Lett.* 271, 278–291. <https://doi.org/10.1016/j.epsl.2008.04.021>

799 Birgel, D., Meister, P., Lundberg, R., Horath, T.D., Bontognali, T.R.R., Bahniuk, A.M., de Rezende, C.E.,
800 Vasconcelos, C., McKenzie, J.A., 2015. Methanogenesis produces strong ^{13}C enrichment in

801 stromatolites of Lagoa Salgada, Brazil: a modern analogue for Palaeo-/Neoproterozoic stromatolites?
802 *Geobiology* 13, 245–266. <https://doi.org/10.1111/gbi.12130>

803 Briones, E.E., Alcocer, J., Cienfuegos, E., Morales, P., 1998. Carbon stable isotopes ratios of pelagic
804 and littoral communities in Alchichica crater-lake, Mexico. *Int. J. Salt Lake Res.* 7, 345–355.
805 <https://doi.org/10.1007/BF02442143>

806 Buchan, A., LeCleir, G.R., Gulvik, C.A., González, J.M., 2014. Master recyclers: features and functions
807 of bacteria associated with phytoplankton blooms. *Nat. Rev. Microbiol.* 12, 686–698.
808 <https://doi.org/10.1038/nrmicro3326>

809 Cadeau, P., Jézéquel, D., Leboulanger, C., Fouilland, E., Le Floc’h, E., Chaduteau, C., Milesi, V.,
810 Guélard, J., Sarazin, G., Katz, A., d’Amore, S., Bernard, C., Ader, M., 2020. Carbon isotope evidence for
811 large methane emissions to the Proterozoic atmosphere. *Sci. Rep.* 10, 18186.
812 <https://doi.org/10.1038/s41598-020-75100-x>

813 Cai, C., Li, K., Liu, D., John, C.M., Wang, D., Fu, B., Fakhraee, M., He, H., Feng, L., Jiang, L., 2021.
814 Anaerobic oxidation of methane by Mn oxides in sulfate-poor environments. *Geology* 49, 761–766.
815 <https://doi.org/10.1130/G48553.1>

816 Callieri, C., Coci, M., Corno, G., Macek, M., Modenutti, B., Balseiro, E., Bertoni, R., 2013. Phylogenetic
817 diversity of nonmarine picocyanobacteria. *FEMS Microbiol. Ecol.* 85, 293–301.
818 <https://doi.org/10.1111/1574-6941.12118>

819 Carrasco-Núñez, G., Ort, M.H., Romero, C., 2007. Evolution and hydrological conditions of a maar
820 volcano (Atexcac crater, Eastern Mexico). *J. Volcanol. Geotherm. Res.* 159, 179–197.
821 <https://doi.org/10.1016/j.jvolgeores.2006.07.001>

822 Chako Tchamabé, B., Carrasco-Núñez, G., Miggins, D.P., Németh, K., 2020. Late Pleistocene to
823 Holocene activity of Alchichica maar volcano, eastern Trans-Mexican Volcanic Belt. *J. South Am. Earth*
824 *Sci.* 97, 102404. <https://doi.org/10.1016/j.jsames.2019.102404>

825 Cheng, C., Zhang, J., He, Q., Wu, H., Chen, Y., Xie, H., Pavlostathis, S.G., 2021. Exploring simultaneous
826 nitrous oxide and methane sink in wetland sediments under anoxic conditions. *Water Res.* 194,
827 116958. <https://doi.org/10.1016/j.watres.2021.116958>

828 Close, H.G., Henderson, L.C., 2020. Open-Ocean Minima in $\delta^{13}\text{C}$ Values of Particulate Organic Carbon
829 in the Lower Euphotic Zone. *Front. Mar. Sci.* 7, 540165. <https://doi.org/10.3389/fmars.2020.540165>

830 Crowe, S.A., Katsev, S., Leslie, K., Sturm, A., Magen, C., Nomosatryo, S., Pack, M.A., Kessler, J.D.,
831 Reeburgh, W.S., Roberts, J.A., González, L., Douglas Haffner, G., Mucci, A., Sundby, B., Fowle, D.A.,
832 2011. The methane cycle in ferruginous Lake Matano: Methane cycle in ferruginous Lake Matano.
833 *Geobiology* 9, 61–78. <https://doi.org/10.1111/j.1472-4669.2010.00257.x>

834 Dean, W.E., Gorham, E., 1998. Magnitude and significance of carbon burial in lakes, reservoirs, and
835 peatlands. *Geology* 26, 535. [https://doi.org/10.1130/0091-7613\(1998\)026<0535:MASOCB>2.3.CO;2](https://doi.org/10.1130/0091-7613(1998)026<0535:MASOCB>2.3.CO;2)

836 Descolas-Gros, C., Fontungne, M., 1990. Stable carbon isotope fractionation by marine
837 phytoplankton during photosynthesis. *Plant Cell Environ.* 13, 207–218.
838 <https://doi.org/10.1111/j.1365-3040.1990.tb01305.x>

839 Emrich, K., Ehhalt, D.H., Vogel, J.C., 1970. Carbon isotope fractionation during the precipitation of
840 calcium carbonate. *Earth Planet. Sci. Lett.* 8, 363–371. [https://doi.org/10.1016/0012-821X\(70\)90109-](https://doi.org/10.1016/0012-821X(70)90109-3)
841 3

842 Ferrari, L., Orozco-Esquivel, T., Manea, V., Manea, M., 2012. The dynamic history of the Trans-
843 Mexican Volcanic Belt and the Mexico subduction zone. *Tectonophysics* 522–523, 122–149.
844 <https://doi.org/10.1016/j.tecto.2011.09.018>

845 Fogel, M.L., Cifuentes, L.A., 1993. Isotope Fractionation during Primary Production, in: Engel, M.H.,
846 Macko, S.A. (Eds.), *Organic Geochemistry, Topics in Geobiology*. Springer US, Boston, MA, pp. 73–98.
847 https://doi.org/10.1007/978-1-4615-2890-6_3

848 Friese, A., Bauer, K., Glombitza, C., Ordoñez, L., Ariztegui, D., Heuer, V.B., Vuillemin, A., Henny, C.,
849 Nomosatryo, S., Simister, R., Wagner, D., Bijaksana, S., Vogel, H., Melles, M., Russell, J.M., Crowe,
850 S.A., Kallmeyer, J., 2021. Organic matter mineralization in modern and ancient ferruginous
851 sediments. *Nat. Commun.* 12, 2216. <https://doi.org/10.1038/s41467-021-22453-0>

852 Fry, B., 2021. 13C/12C fractionation by marine diatoms 13.

853 Fry, B., Jannasch, H.W., Molyneaux, S.J., Wirsén, C.O., Muramoto, J.A., King, S., 1991. Stable isotope
854 studies of the carbon, nitrogen and sulfur cycles in the Black Sea and the Cariaco Trench. *Deep Sea*
855 *Res. Part Oceanogr. Res. Pap.* 38, S1003–S1019. [https://doi.org/10.1016/S0198-0149\(10\)80021-4](https://doi.org/10.1016/S0198-0149(10)80021-4)

856 Fulton, J.M., Arthur, M.A., Thomas, B., Freeman, K.H., 2018. Pigment carbon and nitrogen isotopic
857 signatures in euxinic basins. *Geobiology* 16, 429–445. <https://doi.org/10.1111/gbi.12285>

858 Furian, S., Martins, E.R.C., Parizotto, T.M., Rezende-Filho, A.T., Victoria, R.L., Barbiero, L., 2013.
859 Chemical diversity and spatial variability in myriad lakes in Nhecolândia in the Pantanal wetlands of
860 Brazil. *Limnol. Oceanogr.* 58, 2249–2261. <https://doi.org/10.4319/lo.2013.58.6.2249>

861 Gérard, E., Ménez, B., Couradeau, E., Moreira, D., Benzerara, K., Tavera, R., López-García, P., 2013.
862 Specific carbonate–microbe interactions in the modern microbialites of Lake Alchichica (Mexico).
863 *ISME J.* 7, 1997–2009. <https://doi.org/10.1038/ismej.2013.81>

864 Gonzales-Partida, E., Barragan-R, R.M., Nieva-G, D., 1993. Analisis geoquimico-isotopico de las
865 especies carbonicas del fluido geotermico de Los Humeros, Puebla, México. *Geofis. Int.* 32, 299–309.

866 Gröger, J., Franke, J., Hamer, K., Schulz, H.D., 2009. Quantitative Recovery of Elemental Sulfur and
867 Improved Selectivity in a Chromium-Reducible Sulfur Distillation. *Geostand. Geoanalytical Res.* 33,
868 17–27. <https://doi.org/10.1111/j.1751-908X.2009.00922.x>

869 Gu, B., Schelske, C.L., Hodell, D.A., 2004. Extreme 13C enrichments in a shallow hypereutrophic lake:
870 Implications for carbon cycling. *Limnol. Oceanogr.* 49, 1152–1159.
871 <https://doi.org/10.4319/lo.2004.49.4.1152>

872 Hassan, K.M., 2014. Isotope geochemistry of Swan Lake Basin in the Nebraska Sandhills, USA: Large
873 13C enrichment in sediment-calcite records. *Geochemistry* 74, 681–690.
874 <https://doi.org/10.1016/j.chemer.2014.03.004>

875 Havig, J.R., Hamilton, T.L., McCormick, M., McClure, B., Sowers, T., Wegter, B., Kump, L.R., 2018.
876 Water column and sediment stable carbon isotope biogeochemistry of permanently redox-stratified
877 Fayetteville Green Lake, New York, U.S.A. *Limnol. Oceanogr.* 63, 570–587.
878 <https://doi.org/10.1002/lno.10649>

879 Havig, J.R., McCormick, M.L., Hamilton, T.L., Kump, L.R., 2015. The behavior of biologically important
880 trace elements across the oxic/euxinic transition of meromictic Fayetteville Green Lake, New York,
881 USA. *Geochim. Cosmochim. Acta* 165, 389–406. <https://doi.org/10.1016/j.gca.2015.06.024>

882 Hayes, J.M., Popp, B.N., Takigiku, R., Johnson, M.W., 1989. An isotopic study of biogeochemical
883 relationships between carbonates and organic carbon in the Greenhorn Formation. *Geochim.*
884 *Cosmochim. Acta* 53, 2961–2972. [https://doi.org/10.1016/0016-7037\(89\)90172-5](https://doi.org/10.1016/0016-7037(89)90172-5)

885 Hayes, J.M., Strauss, H., Kaufman, A.J., 1999. The abundance of ¹³C in marine organic matter and
886 isotopic fractionation in the global biogeochemical cycle of carbon during the past 800 Ma. *Chem.*
887 *Geol.* 161, 103–125. [https://doi.org/10.1016/S0009-2541\(99\)00083-2](https://doi.org/10.1016/S0009-2541(99)00083-2)

888 Henkel, J.V., Dellwig, O., Pollehne, F., Herlemann, D.P.R., Leipe, T., Schulz-Vogt, H.N., 2019. A
889 bacterial isolate from the Black Sea oxidizes sulfide with manganese(IV) oxide. *Proc. Natl. Acad. Sci.*
890 116, 12153–12155. <https://doi.org/10.1073/pnas.1906000116>

891 Hurley, S.J., Wing, B.A., Jasper, C.E., Hill, N.C., Cameron, J.C., 2021. Carbon isotope evidence for the
892 global physiology of Proterozoic cyanobacteria. *Sci. Adv.* 7, eabc8998.
893 <https://doi.org/10.1126/sciadv.abc8998>

894 Iniesto, M., Moreira, D., Benzerara, K., Muller, E., Bertolino, P., Tavera, R., López-García, P., 2021a.
895 Rapid formation of mature microbialites in Lake Alchichica, Mexico. *Environ. Microbiol. Rep.* 13, 600–
896 605. <https://doi.org/10.1111/1758-2229.12957>

897 Iniesto, M., Moreira, D., Benzerara, K., Reboul, G., Bertolino, P., Tavera, R., López-García, P., 2022.
898 Planktonic microbial communities from microbialite-bearing lakes sampled along a salinity-alkalinity
899 gradient. *Limnol. Oceanogr. Ino.* 12233. <https://doi.org/10.1002/lno.12233>

900 Iniesto, M., Moreira, D., Reboul, G., Deschamps, P., Benzerara, K., Bertolino, P., Saghai, A., Tavera, R.,
901 López-García, P., 2021b. Core microbial communities of lacustrine microbialites sampled along an
902 alkalinity gradient. *Environ. Microbiol.* 23, 51–68. <https://doi.org/10.1111/1462-2920.15252>

903 Iñiguez, C., Capó-Bauçà, S., Niinemets, Ü., Stoll, H., Aguiló-Nicolau, P., Galmés, J., 2020. Evolutionary
904 trends in RuBisCO kinetics and their co-evolution with CO₂ concentrating mechanisms. *Plant J.* 101,
905 897–918. <https://doi.org/10.1111/tpj.14643>

906 Javoy, M., Pineau, F., Delorme, H., 1986. Carbon and nitrogen isotopes in the mantle. *Chem. Geol.,*
907 *Isotopes in Geology—Picciotto Volume 57*, 41–62. [https://doi.org/10.1016/0009-2541\(86\)90093-8](https://doi.org/10.1016/0009-2541(86)90093-8)

908 Jézéquel, D., Michard, G., Viollier, E., Agrinier, P., Albéric, P., Lopes, F., Abril, G., Bergonzini, L., 2016.
909 Carbon Cycle in a Meromictic Crater Lake: Lake Pavin, France, in: Sime-Ngando, T., Boivin, P.,
910 Chapron, E., Jezequel, D., Meybeck, M. (Eds.), *Lake Pavin: History, Geology, Biogeochemistry, and*
911 *Sedimentology of a Deep Meromictic Maar Lake*. Springer International Publishing, Cham, pp. 185–
912 203. https://doi.org/10.1007/978-3-319-39961-4_11

913 Jiao, N., Herndl, G.J., Hansell, D.A., Benner, R., Kattner, G., Wilhelm, S.W., Kirchman, D.L., Weinbauer,
914 M.G., Luo, T., Chen, F., Azam, F., 2010. Microbial production of recalcitrant dissolved organic matter:
915 long-term carbon storage in the global ocean. *Nat. Rev. Microbiol.* 8, 593–599.
916 <https://doi.org/10.1038/nrmicro2386>

917 Jørgensen, B.B., 1982. Mineralization of organic matter in the sea bed—the role of sulphate
918 reduction. *Nature* 296, 643–645. <https://doi.org/10.1038/296643a0>

919 Karhu, J.A., Holland, H.D., 1996. Carbon isotopes and the rise of atmospheric oxygen. *Geology* 24,
920 867. [https://doi.org/10.1130/0091-7613\(1996\)024<0867:CIATRO>2.3.CO;2](https://doi.org/10.1130/0091-7613(1996)024<0867:CIATRO>2.3.CO;2)

921 Klawonn, I., Van den Wyngaert, S., Parada, A.E., Arandia-Gorostidi, N., Whitehouse, M.J., Grossart,
922 H.-P., Dekas, A.E., 2021. Characterizing the “fungal shunt”: Parasitic fungi on diatoms affect carbon

923 flow and bacterial communities in aquatic microbial food webs. *Proc. Natl. Acad. Sci.* 118,
924 e2102225118. <https://doi.org/10.1073/pnas.2102225118>

925 Knossow, N., Blonder, B., Eckert, W., Turchyn, A.V., Antler, G., Kamyshny, A., 2015. Annual sulfur
926 cycle in a warm monomictic lake with sub-millimolar sulfate concentrations. *Geochem. Trans.* 16, 7.
927 <https://doi.org/10.1186/s12932-015-0021-5>

928 Krissansen-Totton, J., Buick, R., Catling, D.C., 2015. A statistical analysis of the carbon isotope record
929 from the Archean to Phanerozoic and implications for the rise of oxygen. *Am. J. Sci.* 315, 275–316.
930 <https://doi.org/10.2475/04.2015.01>

931 Kuntz, L.B., Laakso, T.A., Schrag, D.P., Crowe, S.A., 2015. Modeling the carbon cycle in Lake Matano.
932 *Geobiology* 13, 454–461. <https://doi.org/10.1111/gbi.12141>

933 Lehmann, M.F., Bernasconi, S.M., Barbieri, A., McKenzie, J.A., 2002. Preservation of organic matter
934 and alteration of its carbon and nitrogen isotope composition during simulated and in situ early
935 sedimentary diagenesis. *Geochim. Cosmochim. Acta* 66, 3573–3584. [https://doi.org/10.1016/S0016-7037\(02\)00968-7](https://doi.org/10.1016/S0016-7037(02)00968-7)

937 Lehmann, M.F., Bernasconi, S.M., McKenzie, J.A., Barbieri, A., Simona, M., Veronesi, M., 2004.
938 Seasonal variation of the δC and δN of particulate and dissolved carbon and nitrogen in Lake Lugano:
939 Constraints on biogeochemical cycling in a eutrophic lake. *Limnol. Oceanogr.* 49, 415–429.
940 <https://doi.org/10.4319/lo.2004.49.2.0415>

941 Lelli, M., Kretzschmar, T.G., Cabassi, J., Doveri, M., Sanchez-Avila, J.I., Gherardi, F., Magro, G., Norelli,
942 F., 2021. Fluid geochemistry of the Los Humeros geothermal field (LHGF - Puebla, Mexico): New
943 constraints for the conceptual model. *Geothermics* 90, 101983.
944 <https://doi.org/10.1016/j.geothermics.2020.101983>

945 Li, H.-C., Ku, T.-L., 1997. $\delta^{13}C$ – $\delta^{18}C$ covariance as a paleohydrological indicator for closed-basin
946 lakes. *Palaeogeogr. Palaeoclimatol. Palaeoecol.* 133, 69–80. [https://doi.org/10.1016/S0031-0182\(96\)00153-8](https://doi.org/10.1016/S0031-0182(96)00153-8)

948 Logan, G.A., Hayes, J.M., Hieshima, G.B., Summons, R.E., 1995. Terminal Proterozoic reorganization
949 of biogeochemical cycles. *Nature* 376, 53–56. <https://doi.org/10.1038/376053a0>

950 Lorenz, V., 1986. On the growth of maars and diatremes and its relevance to the formation of tuff
951 rings. *Bull. Volcanol.* 48, 265–274. <https://doi.org/10.1007/BF01081755>

952 Lugo, A., Alcocer, J., Sánchez, Ma. del R., Escobar, E., Macek, M., 2000. Temporal and spatial variation
953 of bacterioplankton abundance in a tropical, warm-monomictic, saline lake: Alchichica, Puebla,
954 Mexico. *SIL Proc. 1922-2010* 27, 2968–2971. <https://doi.org/10.1080/03680770.1998.11898217>

955 Lugo, A., Alcocer, J., Sanchez, M.R., Escobar, E., 1993. Trophic status of tropical lakes indicated by
956 littoral protozoan assemblages. *SIL Proc. 1922-2010* 25, 441–443.
957 <https://doi.org/10.1080/03680770.1992.11900159>

958 Lyons, T.W., Reinhard, C.T., Planavsky, N.J., 2014. The rise of oxygen in Earth's early ocean and
959 atmosphere. *Nature* 506, 307–315. <https://doi.org/10.1038/nature13068>

960 Macek, M., Medina, X.S., Picazo, A., Peštová, D., Reyes, F.B., Hernández, J.R.M., Alcocer, J., Ibarra,
961 M.M., Camacho, A., 2020. Spirostomum teres: A Long Term Study of an Anoxic-Hypolimnion
962 Population Feeding upon Photosynthesizing Microorganisms. *Acta Protozool.* 59, 13–38.
963 <https://doi.org/10.4467/16890027AP.20.002.12158>

- 964 Mason, E., Edmonds, M., Turchyn, A.V., 2017. Remobilization of crustal carbon may dominate
965 volcanic arc emissions. *Science* 357, 290–294. <https://doi.org/10.1126/science.aan5049>
- 966 Mendonça, R., Müller, R.A., Clow, D., Verpoorter, C., Raymond, P., Tranvik, L.J., Sobek, S., 2017.
967 Organic carbon burial in global lakes and reservoirs. *Nat. Commun.* 8, 1694.
968 <https://doi.org/10.1038/s41467-017-01789-6>
- 969 Mercedes-Martín, R., Ayora, C., Tritlla, J., Sánchez-Román, M., 2019. The hydrochemical evolution of
970 alkaline volcanic lakes: a model to understand the South Atlantic Pre-salt mineral assemblages. *Earth-*
971 *Sci. Rev.* 198, 102938. <https://doi.org/10.1016/j.earscirev.2019.102938>
- 972 Milesi, V.P., Debure, M., Marty, N.C.M., Capano, M., Jézéquel, D., Steefel, C., Rouchon, V., Albéric, P.,
973 Bard, E., Sarazin, G., Guyot, F., Virgone, A., Gaucher, É.C., Ader, M., 2020. Early Diagenesis of
974 Lacustrine Carbonates in Volcanic Settings: The Role of Magmatic CO₂ (Lake Dziani Dzaha, Mayotte,
975 Indian Ocean). *ACS Earth Space Chem.* 4, 363–378.
976 <https://doi.org/10.1021/acsearthspacechem.9b00279>
- 977 Mook, W.G., Bommerson, J.C., Staverman, W.H., 1974. Carbon isotope fractionation between
978 dissolved bicarbonate and gaseous carbon dioxide. *Earth Planet. Sci. Lett.* 22, 169–176.
979 [https://doi.org/10.1016/0012-821X\(74\)90078-8](https://doi.org/10.1016/0012-821X(74)90078-8)
- 980 Mulholland, P.J., Elwood, J.W., 1982. The role of lake and reservoir sediments as sinks in the
981 perturbed global carbon cycle. *Tellus* 34, 490–499. [https://doi.org/10.1111/j.2153-](https://doi.org/10.1111/j.2153-3490.1982.tb01837.x)
982 [3490.1982.tb01837.x](https://doi.org/10.1111/j.2153-3490.1982.tb01837.x)
- 983 O’Leary, M.H., 1988. Carbon Isotopes in Photosynthesis. *BioScience* 38, 328–336.
984 <https://doi.org/10.2307/1310735>
- 985 Pardue, J.W., Scalan, R.S., Van Baalen, C., Parker, P.L., 1976. Maximum carbon isotope fractionation
986 in photosynthesis by blue-green algae and a green alga. *Geochim. Cosmochim. Acta* 40, 309–312.
987 [https://doi.org/10.1016/0016-7037\(76\)90208-8](https://doi.org/10.1016/0016-7037(76)90208-8)
- 988 Peiffer, L., Carrasco-Núñez, G., Mazot, A., Villanueva-Estrada, R.E., Inguaggiato, C., Bernard Romero,
989 R., Rocha Miller, R., Hernández Rojas, J., 2018. Soil degassing at the Los Humeros geothermal field
990 (Mexico). *J. Volcanol. Geotherm. Res.* 356, 163–174.
991 <https://doi.org/10.1016/j.jvolgeores.2018.03.001>
- 992 Petrash, D.A., Steenbergen, I.M., Valero, A., Meador, T.B., Pačes, T., Thomazo, C., 2022. Aqueous
993 system-level processes and prokaryote assemblages in the ferruginous and sulfate-rich bottom
994 waters of a post-mining lake. *Biogeosciences* 19, 1723–1751. [https://doi.org/10.5194/bg-19-1723-](https://doi.org/10.5194/bg-19-1723-2022)
995 [2022](https://doi.org/10.5194/bg-19-1723-2022)
- 996 Pimenov, N.V., Lunina, O.N., Prusakova, T.S., Rusanov, I.I., Ivanov, M.V., 2008. Biological fractionation
997 of stable carbon isotopes at the aerobic/anaerobic water interface of meromictic water bodies.
998 *Microbiology* 77, 751–759. <https://doi.org/10.1134/S0026261708060131>
- 999 Posth, N.R., Bristow, L.A., Cox, R.P., Habicht, K.S., Danza, F., Tonolla, M., Frigaard, N. -U., Canfield,
1000 D.E., 2017. Carbon isotope fractionation by anoxygenic phototrophic bacteria in euxinic Lake
1001 Cadagno. *Geobiology* 15, 798–816. <https://doi.org/10.1111/gbi.12254>
- 1002 Rendon-Lopez, M.J., 2008. *Limnología física del lago crater los Espinos, Municipio de Jiménez*
1003 *Michoacan.*

- 1004 Ridgwell, A., Arndt, S., 2015. Chapter 1 - Why Dissolved Organics Matter: DOC in Ancient Oceans and
1005 Past Climate Change, in: Hansell, D.A., Carlson, C.A. (Eds.), *Biogeochemistry of Marine Dissolved*
1006 *Organic Matter* (Second Edition). Academic Press, Boston, pp. 1–20. [https://doi.org/10.1016/B978-0-](https://doi.org/10.1016/B978-0-12-405940-5.00001-7)
1007 [12-405940-5.00001-7](https://doi.org/10.1016/B978-0-12-405940-5.00001-7)
- 1008 Sackett, W.M., Eckelmann, W.R., Bender, M.L., Bé, A.W.H., 1965. Temperature Dependence of
1009 Carbon Isotope Composition in Marine Plankton and Sediments. *Science* 148, 235–237.
1010 <https://doi.org/10.1126/science.148.3667.235>
- 1011 Saghaï, A., Zivanovic, Y., Moreira, D., Benzerara, K., Bertolino, P., Ragon, M., Tavera, R., López-
1012 Archilla, A.I., López-García, P., 2016. Comparative metagenomics unveils functions and genome
1013 features of microbialite-associated communities along a depth gradient: Comparative metagenomics
1014 of microbialites from Lake Alchichica. *Environ. Microbiol.* 18, 4990–5004.
1015 <https://doi.org/10.1111/1462-2920.13456>
- 1016 Saini, J.S., Hassler, C., Cable, R., Fourquez, M., Danza, F., Roman, S., Tonolla, M., Storelli, N., Jacquet,
1017 S., Zdobnov, E.M., Duhaime, M.B., 2021. Microbial loop of a Proterozoic ocean analogue (preprint).
1018 *Microbiology*. <https://doi.org/10.1101/2021.08.17.456685>
- 1019 Satkoski, A.M., Beukes, N.J., Li, W., Beard, B.L., Johnson, C.M., 2015. A redox-stratified ocean 3.2
1020 billion years ago. *Earth Planet. Sci. Lett.* 430, 43–53. <https://doi.org/10.1016/j.epsl.2015.08.007>
- 1021 Schidlowski, M., 2001. Carbon isotopes as biogeochemical recorders of life over 3.8 Ga of Earth
1022 history: evolution of a concept. *Precambrian Res.* 106, 117–134. [https://doi.org/10.1016/S0301-](https://doi.org/10.1016/S0301-9268(00)00128-5)
1023 [9268\(00\)00128-5](https://doi.org/10.1016/S0301-9268(00)00128-5)
- 1024 Schiff, S.L., Tsuji, J.M., Wu, L., Venkiteswaran, J.J., Molot, L.A., Elgood, R.J., Paterson, M.J., Neufeld,
1025 J.D., 2017. Millions of Boreal Shield Lakes can be used to Probe Archaean Ocean Biogeochemistry.
1026 *Sci. Rep.* 7, 46708. <https://doi.org/10.1038/srep46708>
- 1027 Siebe, C., Guilbaud, M.-N., Salinas, S., Chédeville-Monzo, C., 2012. Eruption of Alberca de los Espinos
1028 tuff cone causes transgression of Zacapu lake ca. 25,000 yr BP in Michoacán, México. Presented at
1029 the IAS 4IMC Conference, Auckland, New Zeland, pp. 74–75.
- 1030 Siebe, C., Guilbaud, M.-N., Salinas, S., Kshirsagar, P., Chevrel, M.O., Jiménez, A.H., Godínez, L., 2014.
1031 Monogenetic volcanism of the Michoacán-Guanajuato Volcanic Field: Maar craters of the Zacapu
1032 basin and domes, shields, and scoria cones of the Tarascan highlands (Paracho-Paricutin region).
1033 Presented at the Pre-meeting field guide for the 5th international Maar Conference, Querétaro,
1034 México, pp. 1–37.
- 1035 Sigala, I., Caballero, M., Correa-Metrio, A., Lozano-García, S., Vázquez, G., Pérez, L., Zawisza, E., 2017.
1036 Basic limnology of 30 continental waterbodies of the Transmexican Volcanic Belt across climatic and
1037 environmental gradients. *Bol. Soc. Geológica Mex.* 69, 313–370.
1038 <https://doi.org/10.18268/BSGM2017v69n2a3>
- 1039 Silva Aguilera, R.A., 2019. Analisis del descenso del nivel de agua del lago Alchichica, Puebla, México
1040 120.
- 1041 Sirevag, R., Buchanan, B.B., Berry, J.A., Troughton, J.H., 1977. Mechanisms of CO₂ Fixation in Bacterial
1042 Photosynthesis Studied by the Carbon Isotope Fractionation Technique. *Arch Microbiol* 112, 4.

- 1043 Sobek, S., Durisch-Kaiser, E., Zurbrügg, R., Wongfun, N., Wessels, M., Pasche, N., Wehrli, B., 2009.
1044 Organic carbon burial efficiency in lake sediments controlled by oxygen exposure time and sediment
1045 source. *Limnol. Oceanogr.* 54, 2243–2254. <https://doi.org/10.4319/lo.2009.54.6.2243>
- 1046 Soetaert, K., Hofmann, A.F., Middelburg, J.J., Meysman, F.J.R., Greenwood, J., 2007. The effect of
1047 biogeochemical processes on pH. *Mar. Chem.* 105, 30–51.
1048 <https://doi.org/10.1016/j.marchem.2006.12.012>
- 1049 Talbot, M.R., 1990. A review of the palaeohydrological interpretation of carbon and oxygen isotopic
1050 ratios in primary lacustrine carbonates. *Chem. Geol. Isot. Geosci. Sect.* 80, 261–279.
1051 [https://doi.org/10.1016/0168-9622\(90\)90009-2](https://doi.org/10.1016/0168-9622(90)90009-2)
- 1052 Thomas, P.J., Boller, A.J., Satagopan, S., Tabita, F.R., Cavanaugh, C.M., Scott, K.M., 2019. Isotope
1053 discrimination by form IC RubisCO from *Ralstonia eutropha* and *Rhodobacter sphaeroides*,
1054 metabolically versatile members of ‘*Proteobacteria*’ from aquatic and soil habitats. *Environ.*
1055 *Microbiol.* 21, 72–80. <https://doi.org/10.1111/1462-2920.14423>
- 1056 Ussiri, D.A.N., Lal, R., 2017. Carbon Sequestration for Climate Change Mitigation and Adaptation.
1057 Springer International Publishing, Cham. <https://doi.org/10.1007/978-3-319-53845-7>
- 1058 Van Mooy, B.A.S., Keil, R.G., Devol, A.H., 2002. Impact of suboxia on sinking particulate organic
1059 carbon: Enhanced carbon flux and preferential degradation of amino acids via denitrification.
1060 *Geochim. Cosmochim. Acta* 66, 457–465. [https://doi.org/10.1016/S0016-7037\(01\)00787-6](https://doi.org/10.1016/S0016-7037(01)00787-6)
- 1061 Vilaclara, G., Chávez, M., Lugo, A., González, H., Gaytán, M., 1993. Comparative description of crater-
1062 lakes basic chemistry in Puebla State, Mexico. *SIL Proc.* 1922-2010 25, 435–440.
1063 <https://doi.org/10.1080/03680770.1992.11900158>
- 1064 Vliet, D.M., Meijerfeldt, F.A.B., Dutilh, B.E., Villanueva, L., Sinninghe Damsté, J.S., Stams, A.J.M.,
1065 Sánchez-Andrea, I., 2021. The bacterial sulfur cycle in expanding dysoxic and euxinic marine waters.
1066 *Environ. Microbiol.* 23, 2834–2857. <https://doi.org/10.1111/1462-2920.15265>
- 1067 Vuillemin, A., Friese, A., Alawi, M., Henny, C., Nomosatryo, S., Wagner, D., Crowe, S.A., Kallmeyer, J.,
1068 2016. Geomicrobiological Features of Ferruginous Sediments from Lake Towuti, Indonesia. *Front.*
1069 *Microbiol.* 7. <https://doi.org/10.3389/fmicb.2016.01007>
- 1070 Wang, S., Yeager, K.M., Lu, W., 2016. Carbon isotope fractionation in phytoplankton as a potential
1071 proxy for pH rather than for [CO₂(aq)]: Observations from a carbonate lake. *Limnol. Oceanogr.* 61,
1072 1259–1270. <https://doi.org/10.1002/lno.10289>
- 1073 Werne, J.P., Hollander, D.J., 2004. Balancing supply and demand: controls on carbon isotope
1074 fractionation in the Cariaco Basin (Venezuela) Younger Dryas to present. *Mar. Chem.* 92, 275–293.
1075 <https://doi.org/10.1016/j.marchem.2004.06.031>
- 1076 Whiticar, M.J., Faber, E., Schoell, M., 1986. Biogenic methane formation in marine and freshwater
1077 environments: CO₂ reduction vs. acetate fermentation—Isotope evidence. *Geochim. Cosmochim.*
1078 *Acta* 50, 693–709. [https://doi.org/10.1016/0016-7037\(86\)90346-7](https://doi.org/10.1016/0016-7037(86)90346-7)
- 1079 Williams, P.M., Gordon, L.I., 1970. Carbon-13: carbon-12 ratios in dissolved and particulate organic
1080 matter in the sea. *Deep Sea Res. Oceanogr. Abstr.* 17, 19–27. [https://doi.org/10.1016/0011-](https://doi.org/10.1016/0011-7471(70)90085-9)
1081 [7471\(70\)90085-9](https://doi.org/10.1016/0011-7471(70)90085-9)

- 1082 Wittkop, C., Teranes, J., Lubenow, B., Dean, W.E., 2014. Carbon- and oxygen-stable isotopic
1083 signatures of methanogenesis, temperature, and water column stratification in Holocene siderite
1084 varves. *Chem. Geol.* 389, 153–166. <https://doi.org/10.1016/j.chemgeo.2014.09.016>
- 1085 Zeyen, N., Benzerara, K., Beyssac, O., Daval, D., Muller, E., Thomazo, C., Tavera, R., López-García, P.,
1086 Moreira, D., Duprat, E., 2021. Integrative analysis of the mineralogical and chemical composition of
1087 modern microbialites from ten Mexican lakes: What do we learn about their formation? *Geochim.*
1088 *Cosmochim. Acta* 305, 148–184. <https://doi.org/10.1016/j.gca.2021.04.030>
- 1089 Zohary, T., Erez, J., Gophen, M., Berman-Frank, I., Stiller, M., 1994. Seasonality of stable carbon
1090 isotopes within the pelagic food web of Lake Kinneret. *Limnol. Oceanogr.* 39, 1030–1043.
1091 <https://doi.org/10.4319/lo.1994.39.5.1030>
- 1092 Zyakun, A.M., Lunina, O.N., Prusakova, T.S., Pimenov, N.V., Ivanov, M.V., 2009. Fractionation of
1093 stable carbon isotopes by photoautotrophically growing anoxygenic purple and green sulfur bacteria.
1094 *Microbiology* 78, 757–768. <https://doi.org/10.1134/S0026261709060137>
- 1095